© 2017. Published by The Company of Biologists Ltd | Development (2017) 144, 3547-3561 doi:10.1242/dev.152686

RESEARCH ARTICLE

HOXA5 plays tissue-specific roles in the developing respiratory system

Kim Landry-Truchon[1], Nicolas Houde[1], Olivier Boucherat[1,*], France-Hélène Joncas[1], Jeremy S. Dasen[2], Polyxeni Philippidou[2,‡], Jennifer H. Mansfield[3] and Lucie Jeannotte[1,§]

ABSTRACT

Hoxa5 is essential for development of several organs and tissues. In the respiratory system, loss of *Hoxa5* function causes neonatal death due to respiratory distress. Expression of HOXA5 protein in mesenchyme of the respiratory tract and in phrenic motor neurons of the central nervous system led us to address the individual contribution of these *Hoxa5* expression domains using a conditional gene targeting approach. *Hoxa5* does not play a cell-autonomous role in lung epithelium, consistent with lack of HOXA5 expression in this cell layer. In contrast, ablation of *Hoxa5* in mesenchyme perturbed trachea development, lung epithelial cell differentiation and lung growth. Further, deletion of *Hoxa5* in motor neurons resulted in abnormal diaphragm innervation and musculature, and lung hypoplasia. It also reproduced the neonatal lethality observed in null mutants, indicating that the defective diaphragm is the main cause of impaired survival at birth. Thus, *Hoxa5* possesses tissue-specific functions that differentially contribute to the morphogenesis of the respiratory tract.

KEY WORDS: *Hoxa5*, Respiratory system development, Lung, Trachea, Diaphragm, Mouse

INTRODUCTION

In mammals, successful transition to air breathing at birth requires harmonious development of the respiratory system, a highly orchestrated process that involves the synchronized formation of trachea, lung and diaphragm. In the mouse, respiratory development initiates around embryonic day (E) 9 with the outpocketing and elongation of the foregut endoderm into the surrounding mesenchyme to form the laryngotracheal groove and primary lung buds (Morrisey and Hogan, 2010). Next, a coordinated program of dichotomous branching gives rise to the airway tree. Transition from branching morphogenesis to differentiation of the respiratory epithelium into specialized cell types, regionally distributed along the proximo-distal axis, leads to a patterned respiratory tract (Chang et al., 2013). Functional air–blood barriers form via differentiation of the distal epithelium in close association with the expansion of the vasculature. Lung development ends after birth with formation of alveoli, which increase the gas-exchange surface area to meet the respiratory requirements of the growing organism.

Physical forces and mechanical interactions between the thorax and respiratory tract are involved in lung growth and function. In fluid-filled fetal lungs, distention is maintained by breathing-like movements and by upper airway resistance during apnea (Kotecha, 2000). Genetic defects that perturb the thoracic skeleton, or space-occupying lesions that compress the lungs, like congenital diaphragmatic hernia, can cause pulmonary hypoplasia; this in turn compromises respiratory function and can be lethal (Jay et al., 2007). Lung development also requires innervation of the diaphragm by the phrenic nerves. Diaphragm denervation abolishes fetal breathing movements, which impairs lung growth (Wigglesworth and Desai, 1979; Liggins et al., 1981).

Diaphragm muscle formation involves contributions from several embryonic structures: somites, pleuroperitoneal folds (PPFs), septum transversum and neural tube (Merrell and Kardon, 2013; Merrell et al., 2015). Around E10.5, muscle progenitors delaminate from the hypaxial dermomyotome of the cervical (C) somites C3 to C5 to reach the PPFs, proliferate and spread ventrally and dorsally on the septum transversum to colonize the entire diaphragm, except the tendinous central region. Muscle progenitors then undergo two waves of myogenesis to differentiate into myofibers (Bentzinger et al., 2012). Meanwhile, the phrenic motor neurons exit the neural tube, also from the C3-C5 region, reach the PPFs and split into three primary trunks, the sternocostal, dorsocostal and crural branches, to innervate the entire diaphragm (Merrell and Kardon, 2013). Muscle progenitors and nerves reach the PPFs at the cervical level, and together descend toward the lower thorax as the lung and heart grow within the thoracic cavity (Allan and Greer, 1997). The PPFs, which constitute a transient embryonic structure, ultimately contribute to the diaphragm's central tendon and connective tissue fibroblasts (Merrell et al., 2015).

Respiratory tract morphogenesis relies on the functional integration of several transcriptional regulators and signaling pathways. Together, they direct reciprocal interactions between epithelium and mesenchyme, and control cell proliferation, differentiation and branching (Morrisey and Hogan, 2010; Hogan et al., 2014). Inappropriate expression of regulatory genes can cause malformations and diseases.

In vertebrates, Hox genes occupy a crucial position in the developmental hierarchy. They encode transcription factors that control the formation of body segment-specific structures via downstream effectors that, in turn, direct region-specific morphogenetic events in numerous tissue types along the embryonic axes. In mammals, 39 Hox genes are organized in four clusters and classified into 13 paralog groups. The spatiotemporal profile of Hox expression reflects the organization of clusters, the

[1]Centre de Recherche sur le Cancer de l'Université Laval, CRCHU de Québec, L'Hôtel-Dieu de Québec, Québec G1R 3S3, Canada. [2]NYU Neuroscience Institute, Department of Neuroscience and Physiology, NYU School of Medicine, New York, NY 10036, USA. [3]Department of Biology, Barnard College-Columbia University, New York, NY 10027, USA.
*Present address: Centre de recherche de l'Institut Universitaire de cardiologie et de pneumologie de Québec, Québec G1V 4G5, Canada. ‡Present address: Department of Neurosciences, Case Western Reserve University School of Medicine, Cleveland, OH 44106, USA.

§Author for correspondence (lucie.jeannotte@crhdq.ulaval.ca)

L.J., 0000-0001-5578-420X

Received 26 March 2017; Accepted 16 August 2017

Development (2017) 144, 3547-3561 doi:10.1242/dev.152686

3′ most genes being expressed earlier and in more anterior domains than the 5′ located ones (McGinnis and Krumlauf, 1992). Several Hox genes, predominantly from the 3′ half of clusters, are expressed along the respiratory tract, each with distinct proximal-distal distribution (Herriges et al., 2012). Previous work has shown the requirement for the three Hox5 paralog genes in lung development. They are expressed in a partially overlapping pattern: *Hoxa5* and *Hoxb5* are strongly expressed in lung mesenchyme, whereas *Hoxc5* expression is barely detected (Boucherat et al., 2013; Hrycaj et al., 2015). *Hoxa5* and *Hoxc5*, but not *Hoxb5*, are expressed in the phrenic motor neurons, which innervate the diaphragm (Philippidou et al., 2012). Finally, only *Hoxa5* is expressed in tracheal mesenchyme. In agreement with its numerous expression domains in the developing respiratory system, most *Hoxa5*$^{-/-}$ pups die at birth from respiratory failure, and show tracheal occlusion, lung hypoplasia and cell misspecification, and diaphragm innervation defects (Jeannotte et al., 1993; Aubin et al., 1997; Boucherat et al., 2013). In contrast, *Hoxb5* and *Hoxc5* single mutants are viable. The lung phenotypic traits of *Hoxb5* mutants are less severe than for *Hoxa5* mutants, whereas *Hoxc5* mutants lack respiratory defects (Boucherat et al., 2013; P.P. and L.J., unpublished). These data unveil the functional predominance of *Hoxa5* in formation of the respiratory system. They also show that *Hoxa5* can compensate for the lack of Hox5 paralog function, as further supported by the increased *Hoxa5* expression detected in *Hoxb5*$^{-/-}$ lungs (Boucherat et al., 2013). Compound mutants for the three Hox5 genes display an exacerbated lung phenotype, likely reflecting functional redundancy due to expression overlap (Hrycaj et al., 2015).

The functions of *Hoxa5* in trachea, lung and diaphragm may separately or in combination affect lung formation and neonate survival. To dissect the tissue-specific role(s) of *Hoxa5* in respiratory system development, we used a *Hoxa5* conditional allele with Cre recombinase deleter strains to ablate *Hoxa5* in epithelium, mesenchyme, or motor neurons. Epithelial deletion revealed no role for *Hoxa5* in this tissue, but deletion in either of the latter tissues resulted in hypoplastic lungs. Mesenchymal deletion of *Hoxa5* also reproduced the abnormal patterning of tracheal cartilage and lung cell misspecification seen in *Hoxa5* null mutants. However, only deletion of *Hoxa5* in motor neurons caused death at birth owing to the abnormal innervation and formation of the diaphragm. Thus, the functional prevalence of *Hoxa5* in the formation of the respiratory system results from distinct functions of *Hoxa5* in its different expression sites.

RESULTS

HOXA5 expression in the developing respiratory system

We previously showed that *Hoxa5* mRNA is expressed in the mesenchyme along the entire embryonic respiratory tract (Boucherat et al., 2013). Immunofluorescence assays confirmed HOXA5 protein expression in mesenchymal nuclei of upper airways and distal lung at E12.5 during branching morphogenesis, and also in the developing diaphragm (Fig. 1A,B). Further, descendants of *Hoxa5*-expressing cells showed restricted fates within the diaphragm. We bred a *Hoxa5-Cre* transgenic line with the *R26*^{mT} reporter mouse. *R26*^{mT}-positive cells, corresponding to descendants of *Hoxa5*-expressing cells, were detected in the PPF region of the diaphragm (Bérubé-Simard and Jeannotte, 2014) (Fig. 1C). In the trachea and primary bronchi, HOXA5 protein expression was observed in the ventrolateral mesenchyme (Fig. 1D). HOXA5 distribution in lung and trachea remained similar at later stages (Fig. 1E-F,H-K). As previously shown, HOXA5 immunoreactivity was detected in the prevertebra (pv)3-pv10 region encompassing the domain where diaphragm muscle progenitors originate and phrenic motor column axons exit and project to contact the diaphragm (Fig. 1E,E′) (Coulombe et al., 2010). *Hoxa5*-expressing cells were also present throughout the diaphragm at E14.5 (Fig. 1G-G″). At the end of gestation, *Hoxa5* expression was reduced in the diaphragm, and descendants of *Hoxa5*-expressing cells were observed in the costal region and central tendon (Fig. 1L-M). No co-labeling between *Hoxa5*-expressing or descendant cells and cells positive for the myogenic transcriptional regulator PAX7 was detected in the developing diaphragm, indicating that *Hoxa5* was not expressed in the diaphragm muscle lineage (Fig. S1). In trachea, HOXA5 expression was detected in cartilage condensations and the surrounding mesenchyme at E16.5 and E18.5. In lung, HOXA5 mesenchymal expression became sparser (Fig. 1H-K). HOXA5 protein was also detected in pulmonary endothelial cells (Fig. 1K). HOXA5 expression was not detected in and *Hoxa5* descendants were absent from respiratory epithelium at all stages.

No cell-autonomous role for *Hoxa5* in respiratory epithelium

Although HOXA5 expression appeared to be absent from lung epithelium, it remains possible that expression is too low or restricted for a small cell population to be detected. To exclude a cell-autonomous function in lung epithelium, we ablated *Hoxa5* in epithelium with the *Shh*^{cre} line (Harfe et al., 2004; Boucherat et al., 2014). Immunohistochemistry (IHC) confirmed that HOXA5 expression was not altered in trachea, lung and diaphragm of *Hoxa5*$^{flox/flox}$; *Shh*$^{+/Cre}$ specimens (Fig. S2D-I). Further, no phenotype was apparent in these specimens. Offspring were obtained at expected Mendelian ratios at E18.5 and this ratio was maintained to adulthood (Fig. S3A). No lung hypoplasia was observed (Fig. S3B). Epithelial cell differentiation was normal, as assessed by the abundance and distribution of secretory club cells and type I pneumocytes, two cell types that are reduced in *Hoxa5*$^{-/-}$ mutants (Fig. S3C-F). Other *Hoxa5* null phenotypes, including goblet cell metaplasia and enlarged lung airspaces caused by perturbed myofibroblast localization, were also absent following *Hoxa5* epithelial deletion (Fig. S3G-J) (Mandeville et al., 2006). Altogether, these data confirmed that *Hoxa5* has no cell-autonomous role in respiratory epithelium.

Hoxa5 expression in phrenic motor neurons is crucial for survival at birth

To assess the requirement for *Hoxa5* in respiratory mesenchyme and phrenic motor neurons, we used the *Dermo1*$^{+/cre}$ and *Olig2*$^{+/cre}$ deleter mouse lines, respectively (Yu et al., 2003; Dessaud et al., 2007; *Dermo1* is also known as *Twist2*). Dermo1Cre activity is specific to lung and tracheal mesenchyme (Boucherat et al., 2014). However, the *Dermo1*^{Cre} allele was not effective in the entire developing diaphragm, demonstrated by the lack of reporter staining in the PPFs (Fig. S2A). Cre activity of the *Olig2*$^{+/cre}$ line was restricted to the ventral spinal cord with no expression in skeletal muscle or lung (Fig. S2B,C) (Park et al., 2010a). Olig2Cre efficiently removes *Hoxa5* from motor neurons (Philippidou et al., 2012). Here, we confirmed by IHC and quantitative RT-PCR (qRT-PCR) that it did not alter *Hoxa5* expression in other respiratory tissues (Fig. S2J-L,X,Y). In *Hoxa5*$^{flox/flox}$; *Dermo1*$^{+/Cre}$ embryos, HOXA5 expression was reduced but not abolished in trachea, lung and diaphragm mesenchyme, indicating that the Dermo1Cre was inefficient or not expressed in all mesenchymal cell types (Fig. S2M-O,X,Y). To reduce mesenchymal *Hoxa5* expression further, we generated *Hoxa5*$^{flox/-}$; *Dermo1*$^{+/Cre}$ animals. Near-complete loss of HOXA5 protein expression was

Development (2017) 144, 3547-3561 doi:10.1242/dev.152686

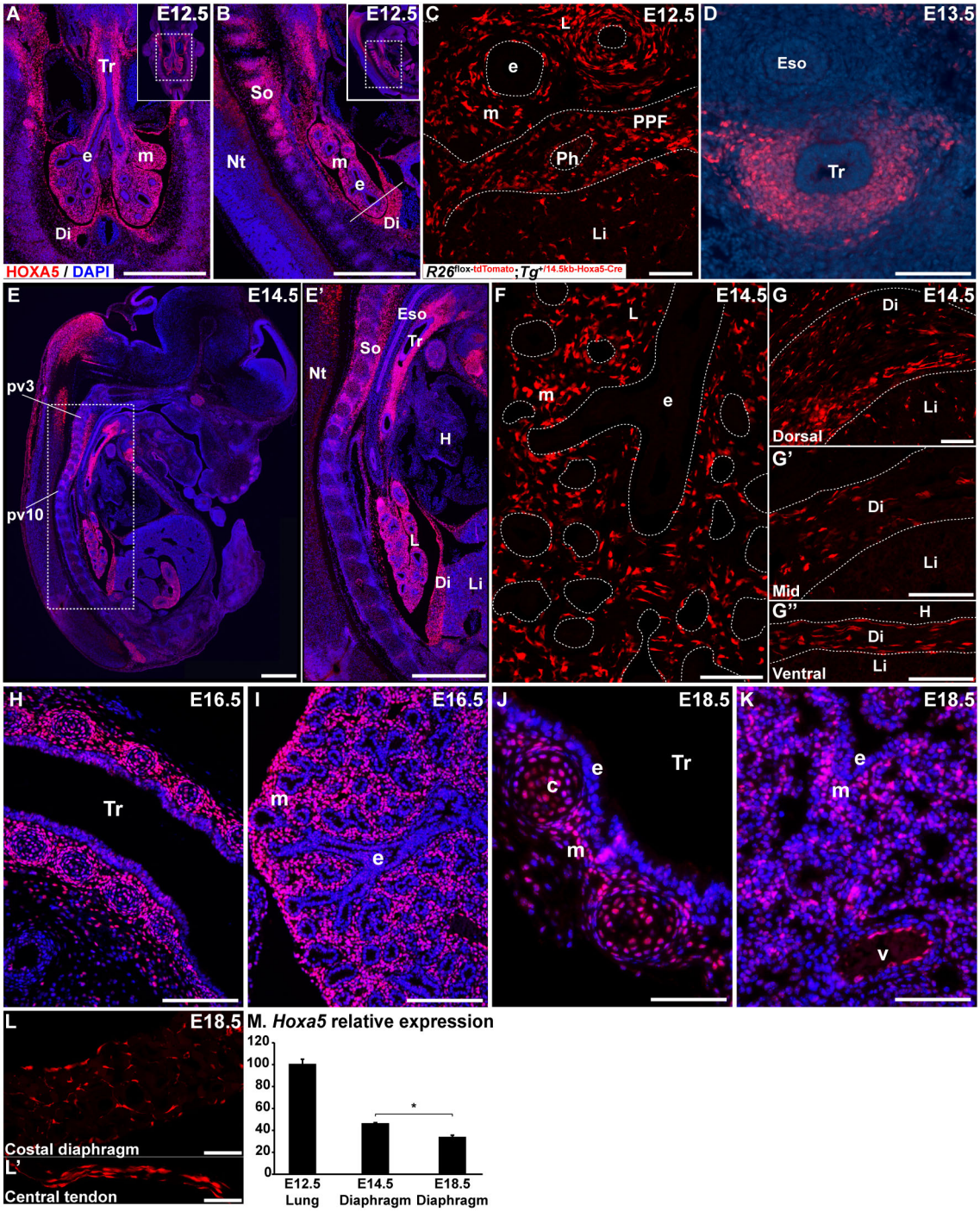

Fig. 1. HOXA5 protein expression in the respiratory system. (A,B,D-E′,H-K) HOXA5 protein was detected by immunofluorescence in mesenchymal nuclei from the trachea, lung and developing diaphragm at E12.5 (A,B), E13.5 (D), E14.5 (E,E′), E16.5 (H,I) and E18.5 (J,K). At E16.5 (H) and E18.5 (J), HOXA5 protein was present in tracheal cartilage cells and surrounding mesenchyme. HOXA5 was also observed in endothelial cells lining lung blood vessels (K). (C,F-G″,L,L′) Cell lineage analysis of *R26*^{mT}; *Hoxa5-Cre* embryos showed *R26*^{mT}-positive cells in lung mesenchyme at E12.5 (C) and E14.5 (F), in the PPF region of developing diaphragm at E12.5 (C) and in diaphragm at E14.5 (G-G″) and E18.5 (L,L′). Frontal (A,H-K), sagittal (B,E-G″,L,L′) and transverse (C,D) sections are shown. The white line in B represents the sectional plan of the PPF region in C. (M) qRT-PCR analysis of *Hoxa5* expression in E12.5 lung and in diaphragm at E14.5 and E18.5. Mean±s.e.m. are shown. **P*<0.05 (Student's *t*-test). c, cartilage; Di, diaphragm; e, epithelium; Eso, esophagus; H, heart; L, lung; Li, liver; m, mesenchyme; Nt, neural tube; Ph, phrenic nerve; pv, prevertebra; So, somites; Tr, trachea; v, vessel. Scale bars: 500 µm (A,B,E,E′); 100 µm (H); 50 µm (C,D,F-G″,I-K); 25 µm (L,L′).

observed in the trachea and lung from these embryos, but it was still detected in the diaphragm (Fig. S2P-Y).

Hoxa5$^{flox/flox}$; *Dermo1*$^{+/Cre}$ and *Hoxa5*$^{flox/-}$; *Dermo1*$^{+/Cre}$ individuals were obtained at expected Mendelian ratios at embryonic and adult ages, suggesting either that the mortality of *Hoxa5*$^{-/-}$ pups did not result from the loss of *Hoxa5* mesenchymal expression or that residual *Hoxa5* expression was sufficient to allow survival (Table 1A,B). Conversely, 45% of the *Hoxa5*$^{flox/flox}$; *Olig2*$^{+/Cre}$ newborns became cyanotic, developed respiratory distress and died within 24 h of birth, indicating that *Hoxa5*

Development (2017) 144, 3547-3561 doi:10.1242/dev.152686

Table 1A. Ratio of genotypes of offspring from *Hoxa5*$^{flox/+}$; *Dermo1*$^{+/Cre}$×*Hoxa5*$^{flox/flox}$

			Dermo1$^{+/+}$		*Dermo1*$^{+/Cre}$	
Age	Number of litters	Total number of offspring	*Hoxa5*$^{flox/+}$	*Hoxa5*$^{flox/flox}$	*Hoxa5*$^{flox/+}$	*Hoxa5*$^{flox/flox}$
E12.5	4	24 (100%)	6 (25%)	9 (37.5%)	3 (12.5%)	6 (25%)
E14.5	6	33 (100%)	10 (30.3%)	10 (30.3%)	7 (21.2%)	6 (18.2%)
E18.5	35	208 (100%)	51 (24.5%)	41 (19.7%)	62 (29.8%)	54 (26%)
P0	10	44 (92%)/4* (8%)	11 (23%)	11 (23%)	8 (17%)/2* (4%)	14 (29%)/2* (4%)
P30	19	75 (100%)	22 (29%)	14 (19%)	22 (29%)	17 (23%)

Table 1B. Ratio of genotypes of offspring from *Hoxa5*$^{flox/+}$; *Dermo1*$^{+/Cre}$×*Hoxa5*$^{flox/flox}$

			Dermo1$^{+/+}$		*Dermo1*$^{+/Cre}$	
Age	Number of litters	Total number of offspring	*Hoxa5*$^{flox/+}$	*Hoxa5*$^{flox/–}$	*Hoxa5*$^{flox/+}$	*Hoxa5*$^{flox/–}$
E18.5	9	41	15 (36.6%)	10 (24.4%)	5 (12.2%)	11 (26.8%)
P0	7	30	7 (23.3%)	7 (23.3%)	7 (23.3%)	9 (30%)
P30	6	22	5 (22.7%)	3 (13.6%)	6 (27.3%)	8 (36.4%)

Table 1C. Ratio of genotypes of offspring from *Hoxa5*$^{flox/+}$; *Dermo1*$^{+/Cre}$×*Hoxa5*$^{flox/flox}$

			Olig2$^{+/+}$		*Olig2*$^{+/Cre}$	
Age	Number of litters	Total number of offspring	*Hoxa5*$^{flox/+}$	*Hoxa5*$^{flox/flox}$	*Hoxa5*$^{flox/+}$	*Hoxa5*$^{flox/flox}$
E12.5	7	50 (100%)	17 (34%)	11 (22%)	11 (22%)	11 (22%)
E14.5	9	58 (100%)	13 (22.4%)	13 (22.4%)	18 (31.1%)	14 (24.1%)
E18.5	28	175 (100%)	40 (22.9%)	48 (27.4%)	41 (23.4%)	46 (26.3%)
P0	13	64 (85%)/11* (15%)	13 (17.3%)/1* (1.3%)	12 (16%)	27 (36%)	12 (16%)/10* (13.4%)
P30	12	65 (100%)	16 (25%)	19 (29%)	21 (32%)	9 (14%)
Expected percentage			**25%**	**25%**	**25%**	**25%**

*Found dead at P0.

deletion in motor neurons was sufficient to reproduce the mortality rate observed for *Hoxa5*$^{-/-}$ pups (Table 1C).

Tracheal cartilage patterning requires *Hoxa5* in mesenchyme

Although *Hoxa5* mesenchymal inactivation was incomplete, it recapitulated several aspects of the *Hoxa5* null phenotype, indicating that a threshold of *Hoxa5* expression is required in the mesenchyme. For example, defects in tracheal cartilage rings are fully penetrant in *Hoxa5*$^{-/-}$ mice (Aubin et al., 1997). Tracheas from controls and *Hoxa5*$^{flox/flox}$; *Olig2*$^{+/Cre}$ were normal (Fig. 2A,B, F,G). Conversely, all *Hoxa5*$^{flox/flox}$; *Dermo1*$^{+/Cre}$ and *Hoxa5*$^{flox/–}$; *Dermo1*$^{+/Cre}$ trachea specimens displayed irregular and incompletely formed cartilaginous rings with abnormal lateral fusion and merging of the cricoid cartilage with the first cartilage rings, anomalies that phenocopy those encountered in *Hoxa5*$^{-/-}$ mice (Fig. 2C-E,H,I). Mesenchymal deletion of *Hoxa5* shared additional phenotypes with *Hoxa5*$^{-/-}$ embryos including ectopic cartilage dots in lungs (Fig. 2C,D), and reduced tracheal length, external diameter and luminal surface (Fig. 2J-L) (Boucherat et al., 2013). Thus, *Hoxa5* activity in mesenchyme, but not in motor neurons, is essential for tracheal cartilage patterning.

Hoxa5$^{-/-}$ embryos show disorganization of the tracheal epithelial layer at E18.5; however, no quantitative or qualitative variation in club, ciliated, basal and goblet cells was observed (Fig. S4) (Aubin et al., 1997). Smooth muscle cells of the trachealis muscle, derived from the dorsal mesenchyme, appeared normal as detected by αSMA (ACTA2) staining, consistent with lack of *Hoxa5* expression in these cells (Fig. 1D, Fig. S4). Thus, *Hoxa5* mesenchymal expression does not contribute to the dorso-ventral patterning of the trachea or to the epithelial-mesenchymal crosstalk that governs tracheal cell specification.

To characterize the mechanisms underlying the *Hoxa5* tracheal phenotype, we examined expression of SOX9, a key transcriptional regulator of chondrogenesis (Turcatel et al., 2013). In the trachea, SOX9 is first uniformly expressed in the ventrolateral mesenchyme, and then expression becomes segmented in a pattern prefiguring the cartilage rings (Elluru and Whitsett, 2004). In lung, SOX9 expression is restricted to committed distal endodermal progenitor cells (Tian et al., 2011). In E14.5 *Hoxa5*$^{-/-}$ embryos, mesenchymal SOX9 protein expression expanded caudally along the secondary bronchi (Fig. 3A,B). This ectopic SOX9 expression might explain the abnormal cartilage dots in mutant lungs. At E18.5, SOX9 tracheal expression was limited to Alcian Blue-positive cartilage rings in controls and *Hoxa5*$^{flox/flox}$; *Olig2*$^{+/Cre}$ specimens. In *Hoxa5*$^{-/-}$ and *Hoxa5*$^{flox/flox}$; *Dermo1*$^{+/Cre}$ embryos, ectopic SOX9 expression was observed outside of the cartilaginous nodules (Fig. 3C-F′). Expression of cartilage-specific type II collagen, a direct transcriptional target of SOX9, was reduced in *Hoxa5*$^{-/-}$ and *Hoxa5*$^{flox/flox}$; *Dermo1*$^{+/Cre}$ tracheas (Fig. 3G-J) (Lefebvre et al., 1997). qRT-PCR analysis confirmed the decrease in *Col2a1* mRNA levels, which was more substantial in *Hoxa5*$^{-/-}$ specimens probably owing to the residual *Hoxa5* expression in trachea of *Hoxa5*$^{flox/flox}$; *Dermo1*$^{+/Cre}$ mutants (Fig. 3K). qRT-PCR also revealed a significant diminution of *Sox9* expression levels, despite the spatial expansion observed. Consistent with this, expression of *Sox5* and *Sox6*, which are genetically downstream of *Sox9* in cartilage specification and constitute with *Sox9* the chondrogenic regulator trio, was also decreased (Fig. 3K) (Lefebvre et al., 1998).

To characterize further the molecular mechanisms leading to *Sox9* dysregulation and cartilage defects, we next examined other known regulators of tracheal cartilage patterning: *Fgf10*, *Shh, Bmp4*, *Tbx4* and *Tbx5*. Of these, all but *Fgf10* influence *Sox9* expression in tracheal mesenchyme (Arora et al., 2012; Park et al., 2010b; Sala et al., 2011). qRT-PCR showed significantly decreased expression of *Bmp4* in the trachea from *Hoxa5*$^{-/-}$ and *Hoxa5*$^{flox/flox}$; *Dermo1*$^{+/Cre}$ mutants, and similarly displayed reduction of *Id1* and *Id2* expression,

Development (2017) 144, 3547-3561 doi:10.1242/dev.152686

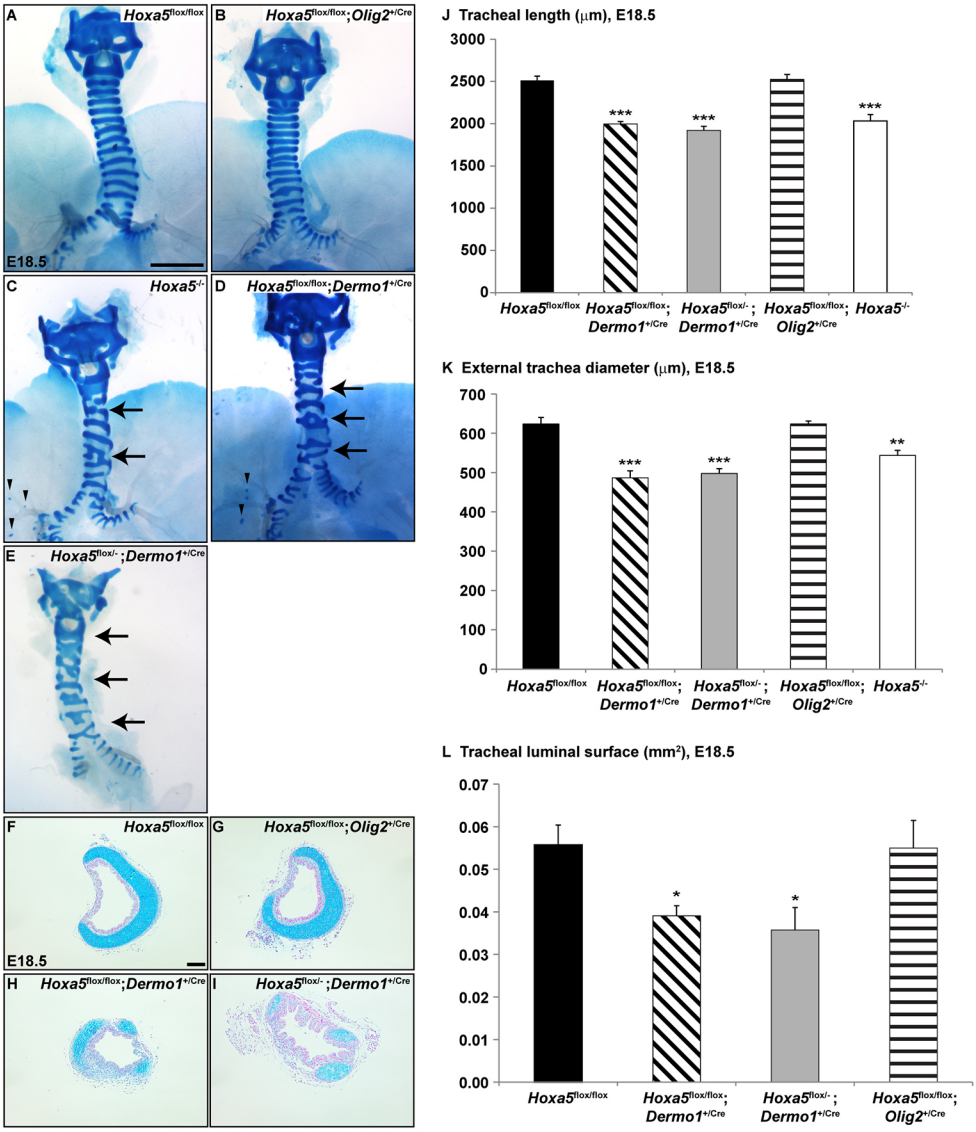

Fig. 2. Mesenchymal *Hoxa5* deletion causes abnormal tracheal cartilage patterning. (A-E) Alcian Blue staining of whole-mount E18.5 tracheas showed cartilage ring malformations (arrows) and ectopic cartilage points (arrowheads) in *Hoxa5*$^{-/-}$ and *Hoxa5*; *Dermo1*$^{+/Cre}$ mutants. (F-I) Cartilage defects and reduced luminal surface were demonstrated by Alcian Blue staining of transverse tracheal sections. (J-L) Morphometric measurements of tracheal length (J), external tracheal diameter (K) and luminal surface (L) were evaluated. Mean±s.e.m. are shown. **P*<0.05, ***P*<0.01, ****P*<0.001 (Student's *t*-test). Scale bars: 1 mm (A-E); 100 µm (F-I).

which are targets of the BMP4 pathway (Fig. S5). Expression of the follistatin-like 1 (*Fstl1*) gene was also diminished in *Hoxa5* mutants. *Fstl1*, which encodes a BMP antagonist, is a direct transcriptional target of HOXA5 in the trachea (Boucherat et al., 2013). No changes in *Fgf10*, *Shh*, *Tbx4* and *Tbx5* expression levels were detected (Fig. S5). These data suggest that *Hoxa5* controls both spatial domain and expression levels of *Sox9* in tracheal mesenchyme via mechanisms that involve BMP signaling. This regulation is cell-autonomous, because conditional deletion of *Hoxa5* in mesenchyme recapitulates the null phenotype. Further, the incomplete deletion by Dermo1Cre indicates that a threshold level of *Hoxa5* is required for its full activity in tracheal mesenchyme.

Lung hypoplasia results from loss of *Hoxa5* in either mesenchyme or motor neurons

Lung hypoplasia, measured as a reduced lung weight/body weight (LW/BW) ratio, occurred in *Hoxa5*$^{flox/flox}$; *Dermo1*$^{+/Cre}$, *Hoxa5*$^{flox/-}$; *Dermo1*$^{+/Cre}$ and *Hoxa5*$^{flox/flox}$; *Olig2*$^{+/Cre}$ mutants and in *Hoxa5*$^{-/-}$ embryos (Fig. 4A). Decreased proliferation contributes to *Hoxa5*$^{-/-}$ lung hypoplasia (Boucherat et al., 2013). A similar downward trend was observed in the number of 5-bromo-2′-deoxyuridine (BrdU)-positive cells in *Hoxa5*$^{flox/flox}$; *Dermo1*$^{+/Cre}$, *Hoxa5*$^{flox/-}$; *Dermo1*$^{+/Cre}$ and *Hoxa5*$^{flox/flox}$; *Olig2*$^{+/Cre}$ lungs (Fig. S6). *Hoxa5* is thus essential in both lung mesenchyme and phrenic motor neurons innervating the diaphragm to sustain correct proliferation of lung tissues.

Proper differentiation of lung epithelium requires *Hoxa5* in mesenchyme

Hoxa5$^{-/-}$ embryos display abnormal and dense lung histology with airway epithelium differentiation defects (Boucherat et al., 2012, 2013). At E18.5, the most affected *Hoxa5*$^{flox/flox}$; *Dermo1*$^{+/Cre}$ and *Hoxa5*$^{flox/-}$; *Dermo1*$^{+/Cre}$ embryos similarly exhibited narrower air spaces and thicker mesenchyme (Fig. 4B-D). Control and *Hoxa5*$^{flox/flox}$; *Olig2*$^{+/Cre}$ lung specimens presented a normal structure with dilated peripheral saccules and thin mesenchyme (Fig. 4B,E). At postnatal day (P) 0, thicker lung mesenchyme persisted in *Hoxa5*$^{flox/flox}$; *Dermo1*$^{+/Cre}$ and *Hoxa5*$^{flox/-}$; *Dermo1*$^{+/Cre}$ specimens but pulmonary structures were expanded (Fig. 4F-H). In contrast, lungs from *Hoxa5*$^{flox/flox}$; *Olig2*$^{+/Cre}$ newborns found dead were collapsed compared with controls, indicating that neuronal *Hoxa5* expression was essential for the expansion of the lung at birth (Fig. 4F,I).

Hoxa5 null mutation causes lung epithelial cell differentiation defects, including fewer club cells and type I pneumocytes

Development (2017) 144, 3547-3561 doi:10.1242/dev.152686

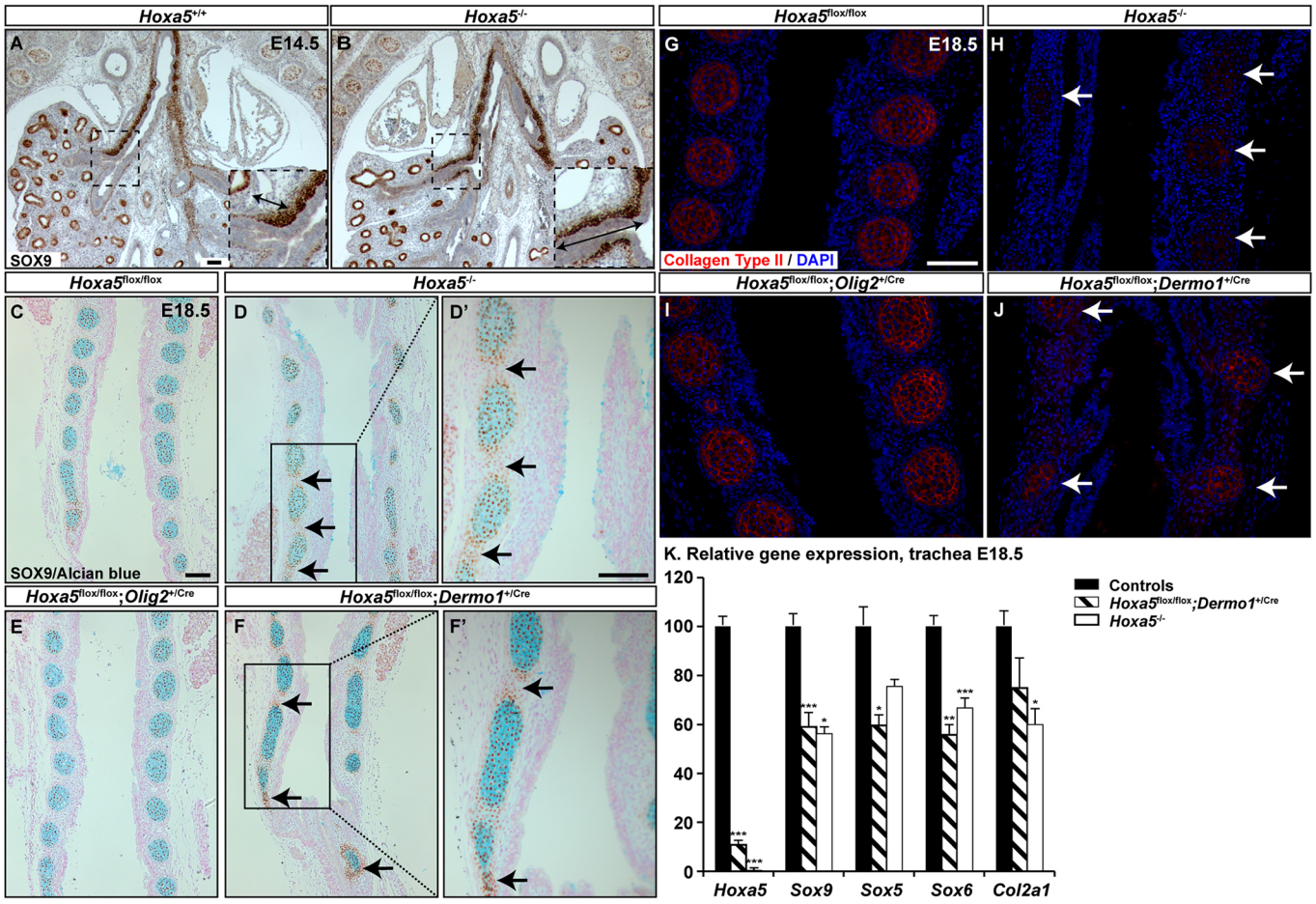

Fig. 3. Mesenchymal *Hoxa5* ablation affects SOX9 spatial expression in trachea. (A,B) SOX9 immunostaining showed ectopic mesenchymal SOX9 expression along the secondary bronchi of E14.5 *Hoxa5*$^{-/-}$ embryos. Insets show higher magnifications of the boxed areas. Double arrows indicate the SOX9 expression domain along the secondary bronchi. (C-F′) SOX9 expression was detected outside of the cartilage nodules in E18.5 *Hoxa5*$^{-/-}$ and *Hoxa5*$^{flox/flox}$; *Dermo1*$^{+/Cre}$ mutants (arrows). (G-J) Collagen type II staining was reduced in *Hoxa5*$^{-/-}$ and *Hoxa5*$^{flox/flox}$; *Dermo1*$^{+/Cre}$ mutants (arrows). (K) qRT-PCR analysis of *Hoxa5*, *Sox9*, *Sox5*, *Sox6* and *Col2a1* expression levels in E18.5 control and *Hoxa5*$^{-/-}$ tracheas. Mean±s.e.m. are shown. *P<0.05, **P<0.01, ***P<0.001 (Student's *t*-test). Scale bars: 100 µm.

(Boucherat et al., 2012, 2013). Both cell types were reduced in *Hoxa5*$^{flox/flox}$; *Dermo1*$^{+/Cre}$ and *Hoxa5*$^{flox/-}$; *Dermo1*$^{+/Cre}$ lungs, but not in control or *Hoxa5*$^{flox/flox}$; *Olig2*$^{+/Cre}$ specimens (Fig. 4J-Q). Goblet cell metaplasia was also observed in *Hoxa5*$^{flox/flox}$; *Dermo1*$^{+/Cre}$ and *Hoxa5*$^{flox/-}$; *Dermo1*$^{+/Cre}$ adult mice whereas mucus-producing cells were scarce in controls and *Hoxa5*$^{flox/flox}$; *Olig2*$^{+/Cre}$ mutants (Fig. 4R-U). Variable expressivity of the lung phenotype in specimens carrying the *Dermo1Cre* allele likely reflects the incomplete activity of the Dermo1Cre. Overall, the requirement for *Hoxa5* in lung epithelial organization and differentiation appears to be mediated by *Hoxa5* activity in mesenchyme, and does not require expression in motor neurons. This further illustrates that *Hoxa5* possesses tissue-specific roles that differentially participate in respiratory tract morphogenesis.

Hoxa5 and *Hoxb5* differentially affect lung regulatory signaling pathways

Deletion of all three Hox5 paralogs in the lung was reported to affect the canonical Wnt/Bmp4 signaling axis but not the Fgf and Shh pathways (Hrycaj et al., 2015). To assess the specific contribution of *Hoxa5* in this context, we evaluated gene expression in *Hoxa5*$^{-/-}$ lungs by qRT-PCR. At E12.5, expression of *Wnt2* and *Wnt7a* was reduced in *Hoxa5*$^{-/-}$ specimens (Fig. S7A). These are ligands of the canonical Wnt pathway expressed in lung mesenchyme and epithelium, respectively (Miller et al., 2012; Hrycaj et al., 2015). Wnt/β-catenin signaling activates the airway smooth muscle program, and acts upstream of Bmp4 and Fgf signaling to regulate differentiation of airway epithelium (Shu et al., 2005; Goss et al., 2011). In *Hoxa5*$^{-/-}$ lungs, expression of downstream targets of the canonical Wnt pathway was significantly decreased, including *Lef1*, a transcriptional effector of the pathway, *Sm22a* (*Tagln*), an early marker of the smooth muscle lineage, and *Pdgfra*, *Fgf10*, *Bmp4* and *Shh*, key players in airway smooth muscle development and branching morphogenesis (Fig. S7A) (Morrisey and Hogan, 2010). At E18.5, expression of *Wnt2*, *Wnt7a*, *Sm22a*, *Pdgfra* and *Fgf10* remained significantly diminished in *Hoxa5*$^{-/-}$ specimens (Fig. S7B). Analysis was also performed on E18.5 *Hoxb5*$^{-/-}$ and compound *Hoxa5*$^{-/-}$; *Hoxb5*$^{-/-}$ mutant embryos. Similar reductions in *Wnt2* and *Fgf10* expression were observed in *Hoxa5* and *Hoxb5* single mutants and in compound mutants. *Wnt7a* expression was not affected in *Hoxb5*$^{-/-}$ specimens but was decreased in *Hoxa5*$^{-/-}$; *Hoxb5*$^{-/-}$ mutants suggesting a predominant contribution of *Hoxa5* to *Wnt7a* expression. In contrast, *Shh* and *Lef1* expression was significantly diminished in *Hoxb5*$^{-/-}$ and *Hoxa5*$^{-/-}$; *Hoxb5*$^{-/-}$ mutants. As in *Hoxa5*$^{-/-}$ lungs,

Development (2017) 144, 3547-3561 doi:10.1242/dev.152686

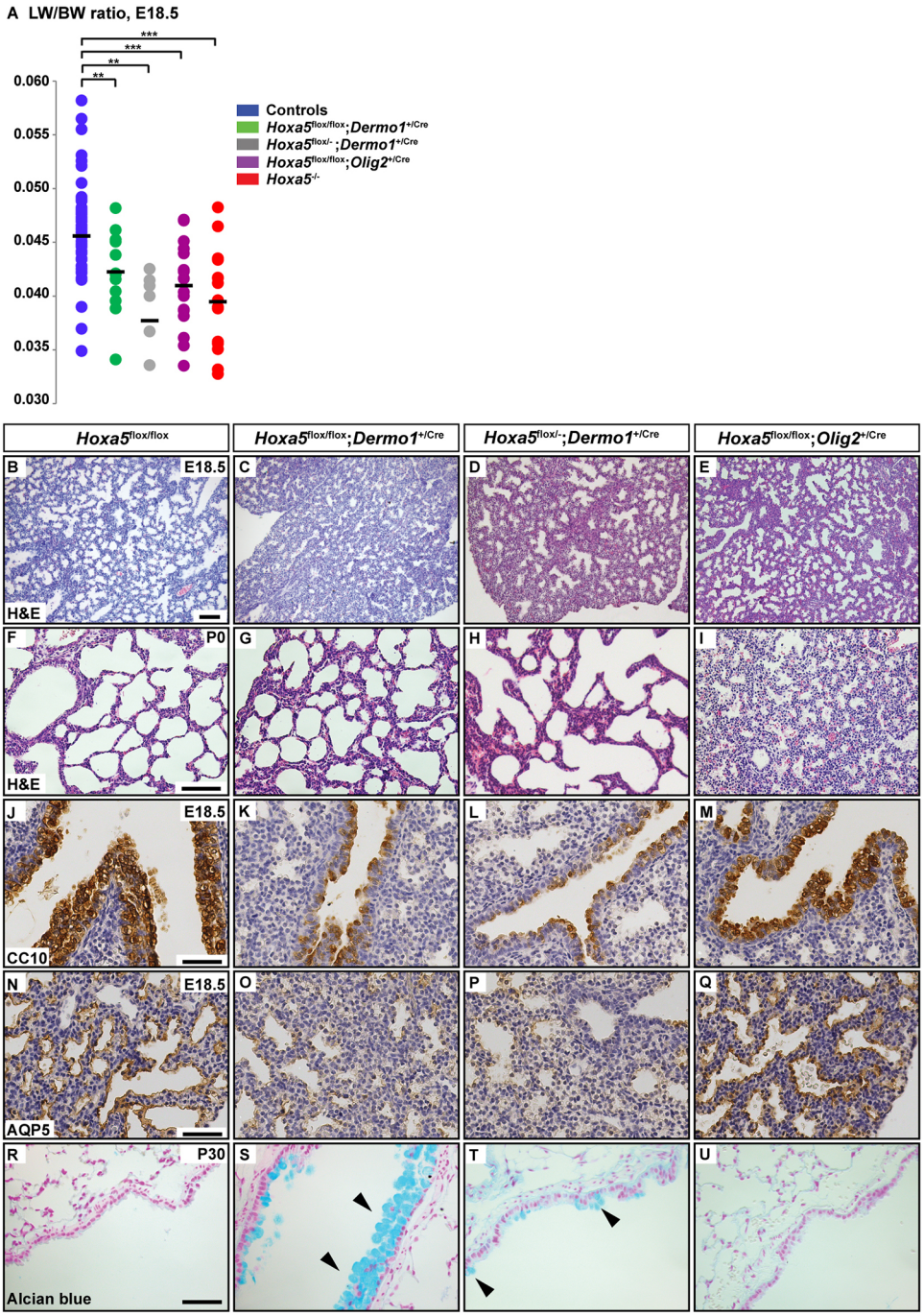

Fig. 4. *Hoxa5* mesenchymal and motor neuron mutations differentially influence lung development. (A) The LW/BW ratio was significantly decreased in E18.5 *Hoxa5*$^{flox/flox}$; *Dermo1*$^{+/Cre}$, *Hoxa5*$^{flox/–}$; *Dermo1*$^{+/Cre}$, *Hoxa5*$^{flox/flox}$; *Olig2*$^{+/Cre}$ and *Hoxa5*$^{–/–}$ embryos versus controls. ***P*<0.01, ****P*<0.001 (Student's *t*-test). (B-E) Comparative histology of lung morphology showed that most affected E18.5 *Hoxa5*$^{flox/flox}$; *Dermo1*$^{+/Cre}$ and *Hoxa5*$^{flox/–}$; *Dermo1*$^{+/Cre}$ lungs exhibited narrower air spaces and thicker mesenchyme compared with *Hoxa5*$^{flox/flox}$ and *Hoxa5*$^{flox/flox}$; *Olig2*$^{+/Cre}$ specimens. (F-I) At P0, *Hoxa5*$^{flox/flox}$; *Olig2*$^{+/Cre}$ lungs were collapsed in contrast to *Hoxa5*$^{flox/flox}$ and *Hoxa5*; *Dermo1*$^{+/Cre}$ specimens. (J-Q) Correct differentiation of club cells and type I pneumocytes, as assessed by CC10 (also known as SCGB1A1) and AQP5 immunostaining, occurred in control and *Hoxa5*$^{flox/flox}$; *Olig2*$^{+/Cre}$ specimens but reduced staining was observed in *Hoxa5*; *Dermo1*$^{+/Cre}$ specimens. (R-U) Goblet cells, detected by Alcian Blue staining, were scarce in control and *Hoxa5*$^{flox/flox}$; *Olig2*$^{+/Cre}$ mice, whereas metaplasia was detected in *Hoxa5*$^{flox/flox}$; *Dermo1*$^{+/Cre}$ and *Hoxa5*$^{flox/–}$; *Dermo*$^{1+/Cre}$ upper airways (arrowheads). Scale bars: 100 µm (B-I); 50 µm (J-U).

Bmp4 expression was unaffected in *Hoxb5*$^{–/–}$ and *Hoxa5*$^{–/–}$; *Hoxb5*$^{–/–}$ mutants. Finally, *Pdgfra*, *Sm22a* and *Acta2* (encoding αSMA) expression was reduced in *Hoxa5*$^{–/–}$ and *Hoxa5*$^{–/–}$; *Hoxb5*$^{–/–}$ but not in *Hoxb5*$^{–/–}$ mutant lungs. Thus, *Hoxa5* and *Hoxb5* genes contribute differentially to fine-tune the signaling networks controlling lung development. They act similarly on the Fgf10 pathway, their influence differs on Wnt/β-catenin and Shh signaling, and *Hoxa5* specifically controls the lung airway smooth muscle program via regulation of *Pdgfra*.

Diaphragm innervation requires *Hoxa5* expression in motor neurons

Almost half of the *Hoxa5*$^{flox/flox}$; *Olig2*$^{+/cre}$ pups died at birth from respiratory distress with compact lungs and a significantly reduced LW/BW ratio, suggesting that lungs failed to grow and inflate normally as a result of impaired fetal breathing movements caused by abnormal diaphragm function. To confirm that this phenotype was associated with abnormal innervation of diaphragm, we characterized phrenic nerves of *Hoxa5*$^{flox/flox}$; *Olig2*$^{+/Cre}$ embryos. The phrenic nerve arises bilaterally from motor neurons in the ventral horns of the cervical spinal cord and contacts the developing diaphragm near the mid-costal region before branching into three primary trunks, of which two extend to innervate the ventral and dorsal parts of diaphragm (Merrell and Kardon, 2013). Whole-mount staining of nerves and neuromuscular junctions revealed that, at E18.5, *Hoxa5*$^{–/–}$ and *Hoxa5*$^{flox/flox}$; *Olig2*$^{+/Cre}$ embryos presented a severely compromised motor innervation pattern. Axons consistently failed to reach the ventral-most part of the

Development (2017) 144, 3547-3561 doi:10.1242/dev.152686

costal muscle, and fewer branches were observed in the dorsal region. Diaphragm innervation was normal in controls and *Hoxa5*$^{flox/flox}$; *Dermo1*$^{+/Cre}$ specimens (Fig. 5A-D). The phenotype was similar at E14.5 suggesting that altered axon patterning, rather than neuronal degeneration, was the cause of the defective innervation (Fig. 5E-G).

Diaphragm muscle formation needs *Hoxa5* expression in motor neurons

Axons typically regulate diaphragm muscle development from the time of initial contact, by facilitating myotube formation via electrically mediated effects and/or diffusible substances. We therefore analyzed the structure of diaphragm muscle fibers in E18.5 embryos by electron microscopy (Greer et al., 1999). Controls and *Hoxa5*$^{flox/flox}$; *Dermo1*$^{+/Cre}$ diaphragms showed aligned sarcomeres. Conversely, *Hoxa5*$^{-/-}$ and *Hoxa5*$^{flox/flox}$; *Olig2*$^{+/Cre}$ mutant specimens presented misaligned Z-discs, damaged sarcomeric proteins and much wider actin-only I-bands, indicative of a high proportion of non-contracted sarcomeres. These defects were observed in the entire muscularized diaphragm (Fig. 6). Further, at E18.5, skeletal muscle was significantly thinner in *Hoxa5*$^{-/-}$ and *Hoxa5*$^{flox/flox}$; *Olig2*$^{+/Cre}$ specimens compared with controls and *Hoxa5*$^{flox/flox}$; *Dermo1*$^{+/Cre}$ embryos (Fig. 7A-E). Both ventral and dorsal regions were equally affected, consistent with electron microscopy data. We also examined muscle fiber size by immunostaining for α-laminin, an extracellular matrix protein of basal lamina, which allows delineation of myofibers. Muscle fiber number per surface area was significantly augmented in *Hoxa5*$^{-/-}$ and *Hoxa5*$^{flox/flox}$; *Olig2*$^{+/Cre}$ diaphragms, reflecting a decrease in myofiber size (Fig. 7F). Moreover, *Hoxa5*$^{-/-}$ and *Hoxa5*$^{flox/flox}$; *Olig2*$^{+/Cre}$ diaphragms showed a decreased number of BrdU-positive nuclei compared with controls and *Hoxa5*$^{flox/flox}$; *Dermo1*$^{+/Cre}$ specimens, indicating that decreased proliferation contributed to muscle atrophy (Fig. 7G).

Muscle atrophy is associated with increased RUNX1 expression, a transcription factor induced in denervated muscle that helps to prevent myofibrillar disorganization and muscle wasting (Zhu et al., 1994; Wang et al., 2005). In *Hoxa5*$^{-/-}$ and *Hoxa5*$^{flox/flox}$; *Olig2*$^{+/Cre}$ diaphragms, *Runx1* expression was significantly increased in response to the incorrect innervation of the diaphragm (Fig. 7H). Thus, even if phrenic nerves reached the dorsal region of the diaphragm in these mutants, neuromuscular contacts appeared to be insufficient to properly support muscular development and growth, causing muscle atrophy. The decreased mechanical forces of the atrophic myofibers in turn likely caused a reduction in fetal breathing-like movements, contributing to lung hypoplasia and resulting in neonatal mortality.

Differentiation of diaphragm muscle fibers requires *Hoxa5* expression in motor neurons

The defective sarcomeres, reduced diaphragm thickness and smaller cross-sectional area of the myofibers in *Hoxa5*$^{-/-}$ and

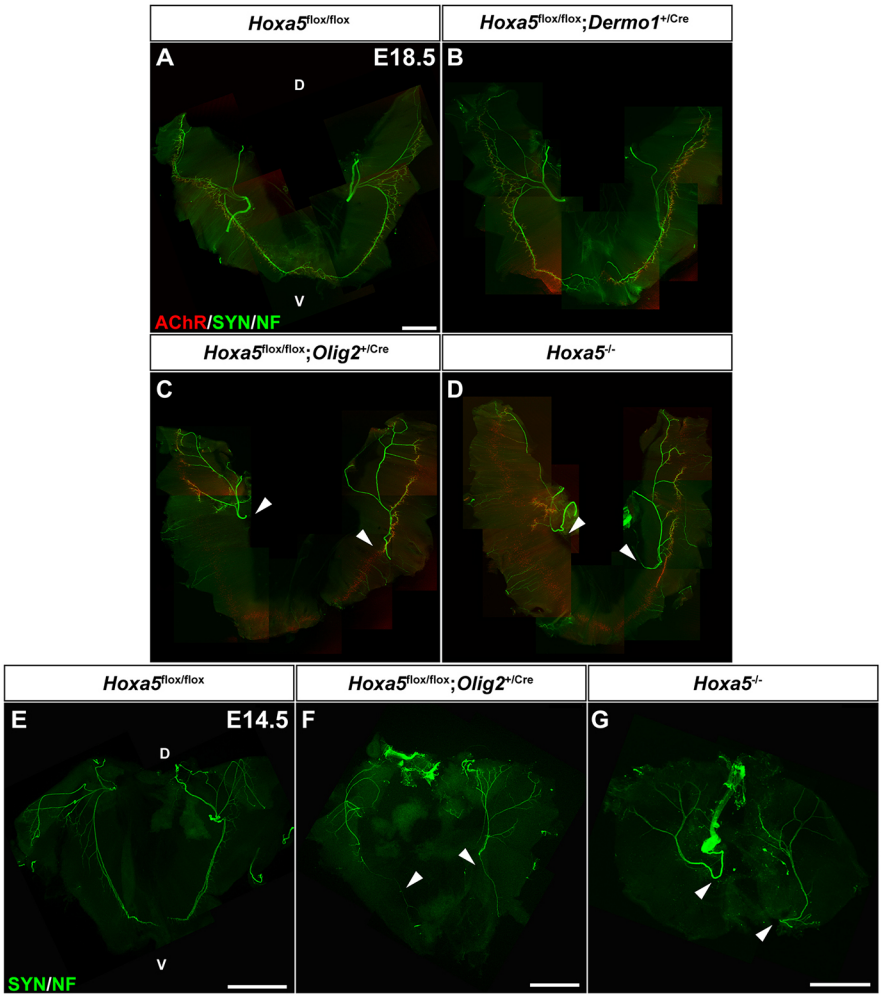

Fig. 5. Abnormal diaphragm innervation in *Hoxa5* motor neuron mutants. (A-G) Analysis of diaphragm innervation patterns at E18.5 (A-D) and E14.5 (E-G) by whole-mount IF staining of neurofilaments (NF), synaptophysin (SYN) and α-bungarotoxin (AChR). Arrowheads indicate failure of phrenic nerves to reach the most ventral part of diaphragm costal muscle at both ages in *Hoxa5*$^{flox/flox}$; *Olig2*$^{+/Cre}$ and *Hoxa5*$^{-/-}$ specimens. Single images covering overlapping portions of the diaphragm muscle were manually stitched together in Photoshop to obtain the composite images of the entire muscle. D, dorsal; V, ventral. Scale bars: 1 mm.

Development (2017) 144, 3547-3561 doi:10.1242/dev.152686

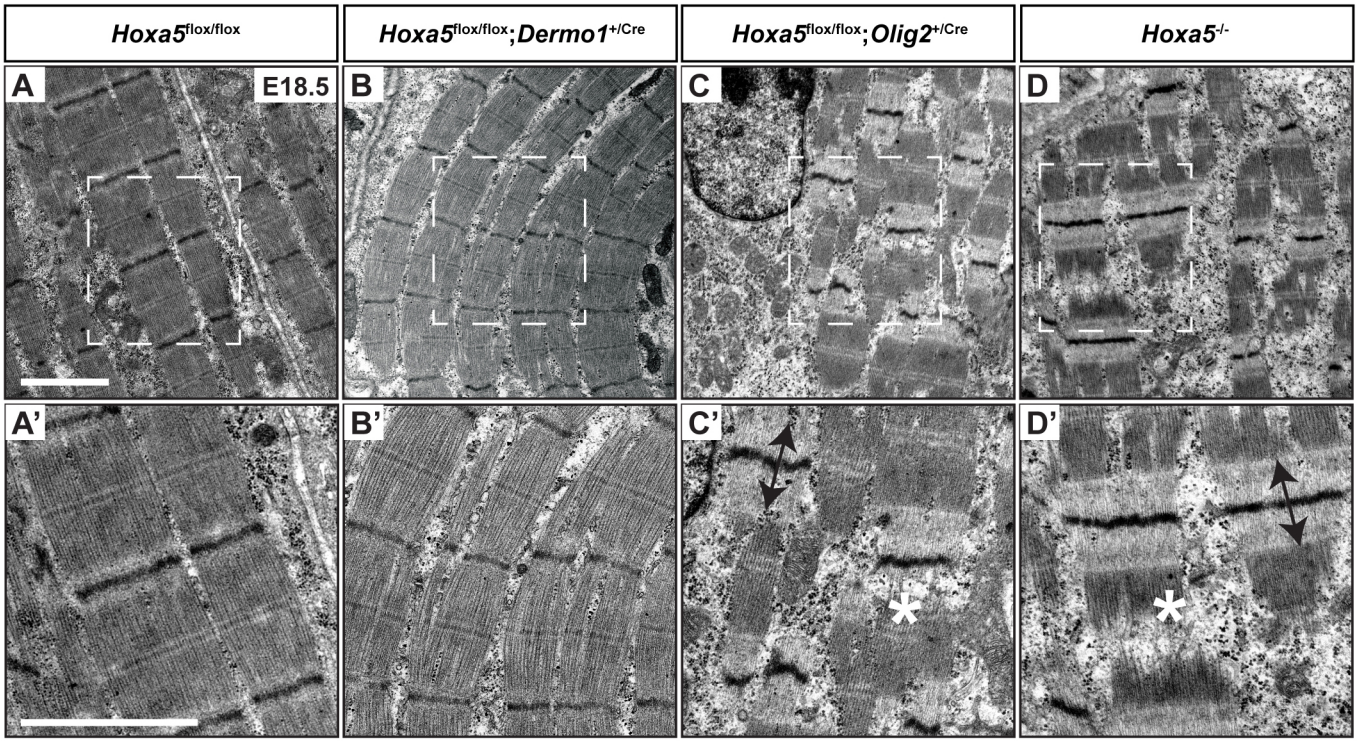

Fig. 6. Electron microscopy analysis of diaphragms from *Hoxa5* mutants. (A-D′) Representative micrographs showing ultrastructure of diaphragms from E18.5 mutant embryos. Controls (A,A′) and *Hoxa5*$^{flox/flox}$; *Dermo1*$^{+/Cre}$ (B,B′) specimens presented normal sarcomeres whereas *Hoxa5*$^{flox/flox}$; *Olig2*$^{+/Cre}$, (C,C′) and *Hoxa5*$^{-/-}$ (D,D′) diaphragms exhibited misaligned sarcomeres with a high proportion of non-contracted myofibers. Asterisks indicate damaged sarcomeric proteins and double arrowheads show wide I-bands. Lower panels show higher magnifications of the boxed areas above. Scale bars: 2 µm.

Hoxa5$^{flox/flox}$; *Olig2*$^{+/Cre}$ embryos raised the question of whether aberrant muscle differentiation contributes to the *Hoxa5* phenotype. We thus analyzed expression of myogenic transcriptional regulators in these two mutants. Somitic myogenic precursors express *Pax3* and *Pax7* and the myogenic regulatory factor (MRF) *Myf5* (Sambasivan and Tajbakhsh, 2007; Bentzinger et al., 2012). Expression of these three genes was significantly reduced in E18.5 *Hoxa5*$^{-/-}$ diaphragms, suggesting defective expansion, migration and/or maintenance of the resident myogenic progenitor population (Fig. 7I). Surprisingly, although *Pax3* and *Myf5* are genetically upstream of the MRF *Myod* (*Myod1*), its expression was significantly augmented in *Hoxa5*$^{-/-}$ specimens (Tajbakhsh et al., 1997). Abnormal expression of both *Myod* and *Myf5* in *Hoxa5*$^{-/-}$ specimens might reflect aberrant progenitor fate decisions. In contrast, expression of the MRFs myogenin (*Myog*) and *Mrf4* (*Myf6*), regulators of myocyte fusion and myotube formation, was unaffected (Fig. 7I). A negative-feedback loop exists between *Myod* and *Igf2* in the diaphragm muscle, and double deletion of these genes causes diaphragm atrophy (Borensztein et al., 2013). Consistently, E18.5 *Hoxa5*$^{-/-}$ diaphragms also showed decreased *Igf2* expression (Fig. 7I). Notably, none of these changes in myogenic regulatory expression was detected in *Hoxa5*$^{flox/flox}$; *Olig2*$^{+/Cre}$ specimens, suggesting an additional role for *Hoxa5* outside of motor neurons in diaphragm myogenesis.

Both *Hoxa5*$^{flox/flox}$; *Olig2*$^{+/Cre}$ and *Hoxa5*$^{-/-}$ diaphragms showed a high proportion of non-contracted sarcomeres. We thus assessed myofiber type composition in these animals. During mouse embryonic diaphragm formation, two populations of fibers are produced in the first wave of myogenesis expressing either *Myh3* and *Myh7* or *Myh3* and *Myh8* myosin heavy chain isoforms, and giving rise to slow-twitch and fast-twitch muscle fibers, respectively. In the second wave, the developing myofibers only express *Myh3* and *Myh8* (Schiaffino and Reggiani, 2011). *Myh7*, *Myh3* and *Myh8* expression was significantly decreased in both *Hoxa5*$^{flox/flox}$; *Olig2*$^{+/Cre}$ and *Hoxa5*$^{-/-}$ diaphragms (Fig. 7J). In contrast, expression of the adult heavy chain isoforms *Myh1* and *Myh2*, which give rise to fast-twitch muscle fibers, presented an upward trend in these specimens. Together, these results suggested that innervation defects resulting from *Hoxa5* deletion in phrenic motor neurons promoted the incorporation of fast-twitch fibers in diaphragm.

DISCUSSION

Hoxa5 is important for the formation of several organs and tissues, consistent with its tissue-specific expression in embryos and adults (Jeannotte et al., 2016). *Hoxa5* is crucial for respiratory system development, and the null mutation disrupts formation of the trachea, lung and diaphragm causing respiratory failure and neonatal death (Aubin et al., 1997; Boucherat et al., 2013). HOXA5 expression is restricted to the mesenchymal layer of the respiratory tract and to the phrenic motor neurons, which are the sole source of diaphragm innervation. The lack of phenotype in *Hoxa5*$^{flox/flox}$; *Shh*$^{+/Cre}$ specimens coupled to immunofluorescence data confirmed that *Hoxa5* is not expressed and has no cell-autonomous function in the respiratory epithelium.

Although *Hoxa5* is not required in lung epithelium, derivatives of both epithelium and mesenchyme are affected by the *Hoxa5* mutation. Indeed, most lung phenotypes are epithelial, indicating that *Hoxa5* acts primarily via mesenchymal-epithelial inductive signaling in this context. Hox5 compound mutants showed that Hox5 genes mainly control the canonical Wnt/Bmp4 signaling axis (Hrycaj et al., 2015). Here, analysis of *Hoxa5* single mutants

Development (2017) 144, 3547-3561 doi:10.1242/dev.152686

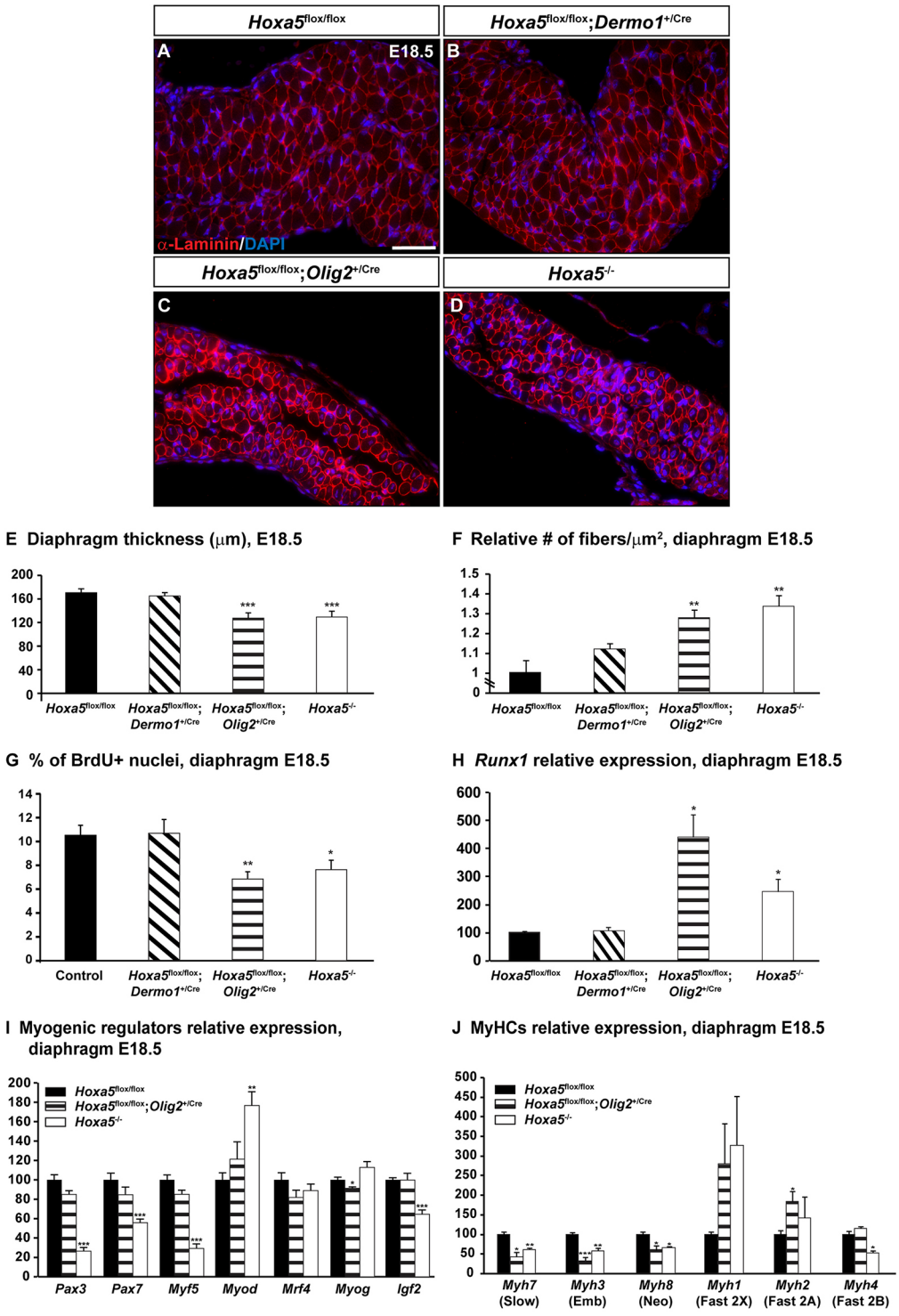

Fig. 7. Diaphragm myogenesis and differentiation requires *Hoxa5* expression in motor neurons. (A-D) α-Laminin immunofluorescence on E18.5 diaphragms delineates myofibers. (E-G) Thickness of the diaphragm (E), number of fibers per surface area (μm^2) to assess myofiber size (F), and percentage of BrdU-positive cells (G) were measured on transverse sections of E18.5 specimens. (H) *Runx1* expression was assessed by qRT-PCR on RNA from E18.5 diaphragms and was shown to be significantly increased in *Hoxa5*$^{flox/flox}$; *Olig2*$^{+/Cre}$ and *Hoxa5*$^{-/-}$ specimens. (I,J) Expression of the myogenic regulators *Pax3*, *Pax7*, *Myf5*, *Mrf4*, *Myog* and *Myod*, and the growth factor *Igf2* (I), and myosin heavy chain isoforms *Myh7*, *Myh3*, *Myh8*, *Myh1*, *Myh2* and *Myh4* (J) in E18.5 *Hoxa5*$^{flox/flox}$, *Hoxa5*$^{flox/flox}$; *Olig2*$^{+/Cre}$ and *Hoxa5*$^{-/-}$ diaphragms was assessed by qRT-PCR. Mean±s.e.m. are shown. *P<0.05, **P<0.01, ***P<0.001 (Student's *t*-test). Emb, embryonic; Neo, neonatal. Scale bar: 50 μm.

establishes the specific contribution of *Hoxa5*. *Hoxa5* positively regulates the canonical Wnt pathway, and also controls expression of *Fgf10*, *Shh* and *Bmp4*, indicating a broad role in signal integration during lung morphogenesis. *Hoxa5* action is also time dependent, as its influence on *Wnt*, *Shh* and *Bmp4* lung expression decreases in older embryos. We previously reported that canonical Wnt activity was increased in adult *Hoxa5*$^{-/-}$ lungs, revealing a difference in how *Hoxa5* controls the Wnt pathway in lung development compared with maintenance (Boucherat et al., 2012). Decreased Wnt activity in the developing lung might underlie the reduced proliferation and resulting lung hypoplasia in *Hoxa5* mutants. Conversely, augmented Wnt activity in adults could explain the increased cell proliferation in lungs from *Hoxa5* surviving mutants, allowing recovery of lung growth (Mandeville et al., 2006).

Hoxa5 positively regulates *Fgf10* lung expression throughout embryogenesis. *Hoxb5* also positively controls *Fgf10* consistent with reduced lung branching in *Hoxb5* mutants (Bellusci et al., 1997; Boucherat et al., 2013). Consequently, *Fgf10* expression was also reduced in *Hoxa5*; *Hoxb5* double mutants. The previously reported lack of *Fgf10* expression change in E14.5 Hox5 triple

Development (2017) 144, 3547-3561 doi:10.1242/dev.152686

mutants is therefore surprising (Hrycaj et al., 2015). One possibility could be negative regulation by the barely expressed *Hoxc5* gene. Alternatively, variation in temporal *Fgf10* expression might exist in Hox5 triple mutants. Finally, the presence of residual trachea tissue in lung samples from the triple mutants could explain the difference, as *Hoxa5* does not regulate *Fgf10* expression in upper airways.

Hoxa5 is the predominant Hox5 paralog to act in the lung airway smooth muscle program, where it regulates *Pdgfra* expression. Alveolar myofibroblasts are interstitial contractile cells responsible for elastin deposition and alveolar formation, two processes affected in *Hoxa5*$^{-/-}$ mutants (Mandeville et al., 2006). They are derived from embryonic lung mesenchyme, which expresses *Pdgfra* and is co-labeled with HOXA5 protein (Lindahl et al., 1997; Hamilton et al., 2003; Mandeville et al., 2006). This suggests a cell-autonomous function for *Hoxa5* in alveolar myofibroblast progenitors (Fig. 8).

Hoxa5 is also involved in lipofibroblast cell fate, as revealed by the reduced expression of peroxisome proliferator-activated receptor gamma (*Pparg*), a master regulator of adipogenesis, and adipose differentiation-related protein (*Adrp*; *Plin2*), a trafficking protein in lipofibroblasts (Fig. S7C, Fig. 8). Both genes are downstream of Fgf10 signaling during lipofibroblast formation (Al Alam et al., 2015). Moreover, the decreased expression of *Tbx4*, an early marker of lung mesenchymal cells, indicates that *Hoxa5* may have a broad impact on lung mesenchymal cell fate, in addition to its instructive role on lung epithelium (Fig. S7C, Fig. 8) (Arora et al., 2012).

Tracheal cartilage malformations are fully penetrant in *Hoxa5*; *Dermo1*$^{+/Cre}$ mice, as in *Hoxa5*$^{-/-}$, indicating that, as with lung development, it is the mesenchymal expression of *Hoxa5* that regulates tracheal development. Incomplete *Hoxa5* deletion by the Dermo1Cre, also establishes the requirement for a minimal level of *Hoxa5* expression. *Hoxb5* and *Hoxc5* cannot rescue the *Hoxa5* tracheal phenotype as they are not expressed in the developing upper airways (Boucherat et al., 2013). Therefore, *Hoxa5* is the only Hox5 paralog gene involved in the tracheal developmental program.

In *Hoxa5* mutants, tracheal cartilage rings form, thus mesenchymal cells become committed towards the chondrogenic lineage. SOX9 and HOXA5 are co-expressed in ventrolateral tracheal mesenchyme. Later, SOX9 becomes restricted to the condensing cartilage rings, whereas HOXA5 is present in ring cartilage and perichondrium and in surrounding mesenchyme (Fig. 1) (Arora et al., 2012). *Hoxa5* mutant tracheas show both altered spatial expression of SOX9, and reduced *Sox9* expression levels. Together, this suggests that *Hoxa5* acts cell-autonomously to control mesenchymal *Sox9* expression, which in turn permits the correct chondrogenesis of cartilage rings. This is consistent with the action of *Hoxa5* on *Sox9* expression during acromion formation and in chick somites, suggesting that it could be a conserved regulatory axis to direct cartilage development and morphology (Aubin et al., 2002; Chen et al., 2013).

Expression of *Bmp4*, and its target genes *Id1* and *Id2*, was decreased in *Hoxa5* mutant tracheas. BMP4 is a pro-chondrogenic

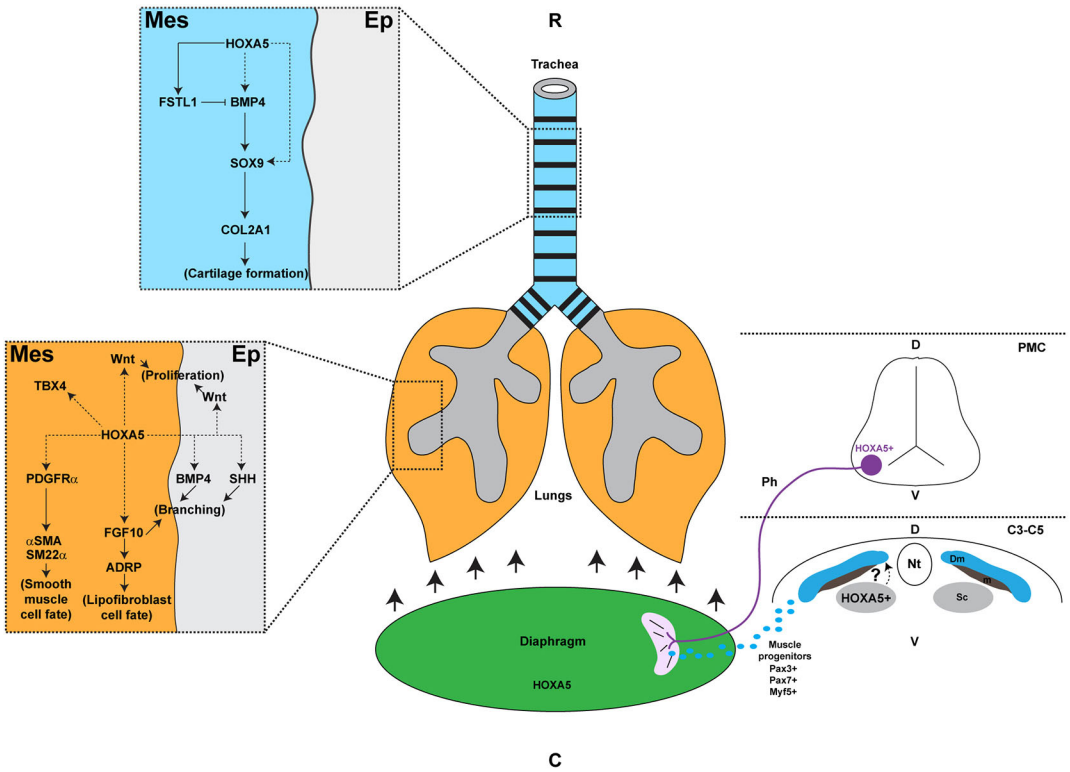

Fig. 8. *Hoxa5* distinct roles in the developing respiratory system. In trachea, HOXA5 expression in mesenchyme directly regulates *Fstl1*, an antagonist of BMP4 signaling. HOXA5 may also control *Bmp4* and *Sox9*, which participate in tracheal cartilage formation. In lung, mesenchymal HOXA5 can activate *Wnt* ligand expression important for cell proliferation, *Fgf10* involved in lung branching and lipofibroblast formation, and *Pdgfra*, essential for smooth muscle cell fate. HOXA5 may also positively control the epithelial expression of *Bmp4* and *Shh* necessary for branching. *Hoxa5* is also expressed in phrenic motor neurons, in the sclerotome of somites from the C3-C5 cervical region and in the diaphragm itself. Loss of *Hoxa5* function in phrenic nerves impairs diaphragm innervation and musculature, which causes lung hypoplasia, respiratory distress and death at birth. The exact role of *Hoxa5* in the diaphragm remains to be determined. C, caudal; C3-C5, cervical somites 3 to 5; D, dorsal; Dm, dermomyotome; Ep, epithelium; m, myotome; Mes, mesenchyme; Nt, neural tube; Ph, phrenic nerve; PMC, phrenic motor column; R, rostral; Sc, sclerotome; V, ventral.

Development (2017) 144, 3547-3561 doi:10.1242/dev.152686

signal that promotes chondrogenesis through *Sox9* activation (Park et al., 2010b). Reduced BMP4 signaling might thus underlie the observed *Sox9* downregulation. Moreover, *Hoxa5* is co-expressed with *Bmp4*, making it a potential direct HOXA5 target (Li et al., 2008). Interestingly, expression of the BMP antagonist *Fstl1* is also reduced in *Hoxa5* mutant specimens, and *Fstl1*$^{-/-}$ mice present a malformed trachea with fewer cartilage rings and a disorganized epithelium reminiscent of the *Hoxa5*$^{-/-}$ tracheal phenotype (Geng et al., 2011). We previously showed that *Fstl1* is a direct HOXA5 transcriptional target (Boucherat et al., 2013). The decreased expression of both *Bmp4* and *Fstl1* following the loss-of-*Hoxa5* function appears to be contradictory. However, it underscores the complexity of the regulatory network in tracheal-bronchial chondrogenesis, which involves extensive cross-regulation between signaling pathways and transcriptional regulators by mechanisms that remain to be fully elucidated (Fig. 8).

Hoxa5$^{flox/flox}$; *Dermo1*$^{+/Cre}$ and *Hoxa5*$^{flox/-}$; *Dermo1*$^{+/Cre}$ adult mice were recovered at the expected Mendelian ratio indicating that tracheal malformations and compact lung architecture are not the cause of lethality of *Hoxa5*$^{-/-}$ newborns. In contrast, *Hoxa5* deletion in phrenic motor neurons reproduced this lethality, demonstrating the crucial importance of *Hoxa5* in diaphragm development and function. Only *Hoxa5* mesenchymal expression appeared to be necessary for lung epithelial cell differentiation. However, both *Hoxa5* mesenchymal and motor neuron mutations caused lung hypoplasia due to decreased proliferation. Thus, *Hoxa5* has tissue-specific functions in mesenchyme and motor neurons that have both converging and distinct effects on respiratory development.

Hoxa5 expression in phrenic motor neurons is essential for diaphragm formation. *Hoxa5*$^{flox/flox}$; *Olig2*$^{+/Cre}$ and *Hoxa5*$^{-/-}$ diaphragms were incorrectly innervated and showed abnormal musculature that evokes diaphragmatic eventration, a condition involving diaphragm relaxation that allows superior displacement of abdominal viscera into the thoracic cavity and impedes lung growth (Ackerman et al., 2012). Abnormal innervation was detected at E14.5, after the division of the phrenic nerve into the three primary branches. The failure of axons to reach the ventral part of the costal muscle, and the absence of recovery during diaphragm development, suggested that the defective innervation originates from axon guidance alterations rather than axonal degeneration and loss of synaptic contacts (Philippidou et al., 2012).

Profound alterations of the muscular component of diaphragm were also observed in *Hoxa5*$^{-/-}$ and *Hoxa5*$^{flox/flox}$; *Olig2*$^{+/Cre}$ specimens, including thinner diaphragm, smaller myofibers and misaligned sarcomeres with damaged proteins, all characteristics of muscle atrophy (Wang et al., 2005; Borensztein et al., 2013). Increased *Runx1* expression, a marker for damaged and regenerating muscle, further supported the notion of muscle atrophy and attempted recovery in *Hoxa5* mutants (Umansky et al., 2015). *Hoxa5*$^{-/-}$ and *Hoxa5*$^{flox/flox}$; *Olig2*$^{+/Cre}$ adult diaphragms presented an irregular distribution of costal muscles restricted to the ventral region (K.L.-T. and L.J., unpublished). This suggests that axon projections present in the dorsal diaphragm, although less abundant, were sufficient to generate synaptic contacts with muscle fibers and allow some muscle rescue.

Diaphragm muscles originate from myogenic precursor cells in the hypaxial dermomyotome of cervical somites C3 to C5, which express the myogenic transcriptional regulators *Pax3*, *Pax7* and *Myf5* (Bentzinger et al., 2012). *Myf5*$^{-/-}$ mice do not present diaphragm defects but *Myf5*; *Myod* double mutants, in which *Mrf4* expression is compromised, lack diaphragm (Braun et al., 1992; Rudnicki et al., 1993; Kassar-Duchossoy et al., 2004). *Splotch* (*Pax3*$^{-/-}$) mutants also lack diaphragm muscle, and that of *Pax7*$^{-/-}$ mice is notably thinner (Tremblay et al., 1998; Seale et al., 2000). Therefore, decreased expression of *Pax3*, *Pax7* and *Myf5* in *Hoxa5*$^{-/-}$ diaphragms might reflect a reduced contribution of myogenic progenitors to the diaphragm musculature.

Interestingly, *Hoxa5*$^{flox/flox}$; *Olig2*$^{+/Cre}$ diaphragms do not show variation in *Pax3*, *Pax7* or *Myf5* expression. Thus, despite morphological similarity between both phenotypes, the diaphragm phenotype of *Hoxa5*$^{-/-}$ mutants might reflect *Hoxa5* activity in cell types other than motor neurons. This could include the diaphragm connective tissue or somite-derived muscles. *Hoxa5* is expressed in the somites from the cervical-thoracic transition domain C3 to T2. However, *Hoxa5* somitic expression is confined to the lateral sclerotome, a source of cartilage and perichondrium, and no expression was detected in the dermomyotome of chicks or myotome of mice (Chen et al., 2013; J.H.M., unpublished). This suggests that the decreased expression of *Pax3*, *Pax7* and *Myf5* in *Hoxa5*$^{-/-}$ diaphragms is unlikely to result from a cell-autonomous action of *Hoxa5* in myotome. However, we cannot exclude an indirect role for *Hoxa5* somitic expression in the selective proliferation, migration and/or survival of myogenic precursors (Fig. 8).

Hoxa5 is also expressed in the developing diaphragm. However, no phenotype was detected in *Hoxa5*$^{flox/flox}$; *Dermo1*$^{+/Cre}$ mutants, possibly owing to the incomplete activity of the *Dermo1*^{Cre} allele in diaphragm. Cell lineage and co-labeling data indicated that *Hoxa5* is not present in muscle cells and is likely expressed in the PPF lineage (Fig. 1, Fig. S1). Thus, other *Cre* deleter mouse lines will have to be tested to determine the role of *Hoxa5* expression in the diaphragm.

Myod expression is positively regulated by both *Pax3* and *Myf5* (Tajbakhsh et al., 1997). However, *Myod* expression was increased in diaphragms from *Hoxa5*$^{-/-}$ mutants. One possible explanation is the decreased expression of *Igf2* also observed in *Hoxa5*$^{-/-}$ diaphragms. *Myod* and *Igf2* show reciprocal negative regulation in this context: *Myod* overexpression compensates for *Igf2* downregulation and *Igf2* overexpression compensates for *Myod* downregulation (Borensztein et al., 2013). The cause of reduced *Igf2* expression in the diaphragm of *Hoxa5*$^{-/-}$ mutants remains unknown.

Myosin heavy chain fast isoform expression is augmented in *Hoxa5*$^{-/-}$ and *Hoxa5*$^{flox/flox}$; *Olig2*$^{+/Cre}$ diaphragms. The fiber composition of a given muscle results from several factors including innervation, mechanical conditions and usage patterns. Moreover, when breathing rate increases, recruitment of fast muscle fibers is favored (Polla et al., 2004). Surviving *Hoxa5*$^{-/-}$ mice present respiratory adaptations including higher breathing frequency and augmented overall minute ventilation to circumvent morphological respiratory system defects (Kinkead et al., 2004). Together, our data suggest that they are compensatory mechanisms to maintain and adapt diaphragm muscle activity in order to allow the survival of *Hoxa5* mutants.

In conclusion, characterization of *Hoxa5* conditional mutants led us to establish that *Hoxa5* regulates respiratory system development via several distinct and tissue-specific functions. These independent expression domains and functions are likely to reflect the stepwise origin and elaboration of respiratory structures in terrestrial vertebrates. For instance, the diaphragm and phrenic motor neurons that innervate it are an evolutionary novelty of mammals, and *Hoxa5* was probably independently recruited for its various functions in the respiratory system as these structures arose (Jung and Dasen, 2015).

Development (2017) 144, 3547-3561 doi:10.1242/dev.152686

MATERIALS AND METHODS

Mouse lines, genotyping and tissue collection

The *Hoxa5* null (*Hoxa5*^{tm1Rob}), *Hoxa5*$^{flox/flox}$ (*Hoxa5*^{tm1Ljea}), 14.5 kb *Hoxa5-cre* [*Tg(Hoxa5-cre)447BLjea*] and *Olig2*^{Cre} [*Olig2*$^{tm1(cre)Tmj}$] mouse lines were previously described (Jeannotte et al., 1993; Dessaud et al., 2007; Tabariès et al., 2007; Bérubé-Simard and Jeannotte, 2014). The *Dermo1*^{Cre} [*Twist2*$^{tm1(cre)Dor}$] line was obtained from Dr Ornitz (Washington University, St. Louis, MO, USA; Yu et al., 2003). The *R26*^{LacZ}, *R26*^{mTmG} and *R26*^{mT} reporter lines [*Gt(ROSA)26Sor*^{tm1Sor}, *Gt(ROSA)26Sor*$^{tm4(ACTB–tdTomato,–EGFP)Luo}$ and *Gt(Rosa)26Sor*$^{tm9(CAG–tdTomato)Hze}$)] and the *Shh*^{Cre} Washington University deleter strain [*Shh*$^{tm1(EGFP/cre)Cjt}$] were purchased (Jackson Laboratory; Soriano, 1999; Harfe et al., 2004; Muzumdar et al., 2007; Madisen et al., 2010). As only individuals carrying the *Hoxa5*$^{–/–}$, *Hoxa5*$^{flox/flox}$; *Dermo1*$^{+/Cre}$, *Hoxa5*$^{flox/–}$; *Dermo1*$^{+/Cre}$ and *Hoxa5*$^{flox/flox}$; *Olig2*$^{+/Cre}$ genotypes presented defects, all other genotypes were referred to as controls except when specified. Mouse lines were maintained in the 129/Sv background. Age of embryos was estimated by considering the morning of the day of the vaginal plug as E0.5. Experimental specimens were genotyped by PCR and Southern blot analyses. Trachea, lung and diaphragm from control and mutant embryos were collected at E12.5, E14.5, E18.5, P0 and P30. The wet lung and body weights were obtained by direct measurement. For RNA extraction, organs were snap-frozen in N_2. Experiments were performed according to the guidelines of Canadian Council on Animal Care and approved by the Institutional Animal Care Committee.

Histology, IHC and immunofluorescence (IF) analyses

Specimens were processed for paraffin (4 µm) or frozen (5-10 µm) sections. Experiments were performed as described (Boucherat et al., 2017). Slides were counterstained with Nuclear Fast Red, Alcian Blue or Hematoxylin. For IF, nuclei were visualized by DAPI staining. The Cyanine 3 Tyramide Signal Amplification Kit (Perkin Elmer) was used at 1/50 dilution for HOXA5 IF detection. Antibodies are listed in Table S1.

β-Galactosidase staining

Detection of β-galactosidase activity in frozen sections (10 µm) from E12.5 embryos was performed as described (Bérubé-Simard and Jeannotte, 2014).

Proliferation assay

Pregnant females were injected intraperitoneally with 100 µg BrdU/g body weight and embryos were collected 1 h later. Proliferation index corresponds to the number of BrdU-immunoreactive cells divided by total cell number for each section analyzed. Four to eight random fields were taken for an average number of 200 diaphragm and 750 lung cells per field, from three to five embryos per genotype.

Electron microscopy

Diaphragms from E18.5 embryos were divided into dorsal-left, dorsal-right, ventral-left and ventral-right regions, fixed in 0.1 M sodium cacodylate, pH7.3, containing 2.5% glutaraldehyde for 24 h, washed in sodium cacodylate buffer, post-fixed in 1% OsO4, dehydrated in ethanol and then propylene oxide, embedded in Epon, and sectioned at 60-80 nm. Sections were stained in 0.4% lead citrate for 8 min and in 3% uranyl acetate solution for 5 min. Pictures were taken with a transmission electron microscope JEOL, JEM1230 (Tokyo, Japan) used at 80 kV and equipped with two CCD cameras: (1) wide-field Gatan Dual Vision and (2) high-resolution Gatan Ultrascan 1000XP.

Alcian Blue cartilage staining

Dissected respiratory tracts from E18.5 embryos were stained overnight at 37°C in 0.015% Alcian Blue, 20% acetic acid prepared in 95% ethanol. Specimens were processed 30 min in 1% KOH for better visualization of cartilage rings.

Morphometric measurements

ImageJ software was used to calculate (1) the tracheal length between the cricoid cartilage and the carina, (2) the trachea external diameter along the most linear portion of trachea, and (3) the number of diaphragm muscle fibers/area (µm^2) at eight dorso-ventral locations in the right costal muscle. Using the Leica SCN 400 F SlideScanner and SlidePath Gateway Software, we measured the tracheal luminal surface, and the diaphragm thickness at eight dorso-ventral locations in the right costal muscle. Three to eleven specimens were used for each genotype tested.

qRT-PCR assays

Total RNA was isolated from trachea, lung and diaphragm of individuals. qRT-PCR experiments were performed as described (Boucherat et al., 2012). Three to eight specimens were used for each genotype tested. Primer sequences are listed in Table S2.

Statistical analyses

Student's *t*-test was performed for comparative studies. A significance level below 5% (P<0.05) was considered statistically significant. Values are expressed as mean±s.e.m. *P<0.05, **P<0.01, ***P<0.001.

Acknowledgements

We thank Drs Jean Charron and Luisa Dandolo for comments, Dr David Ornitz for *Dermo1*^{Cre} mice, Drs Normand Marceau and Gurmukh Singh for antibodies, and Richard Janvier for electron microscopy analysis.

Competing interests

The authors declare no competing or financial interests.

Author contributions

Conceptualization: K.L.-T., O.B., L.J.; Methodology: K.L.-T., N.H., O.B., F.-H.J., P.P., L.J.; Validation: K.L.-T., N.H., O.B., F.-H.J., P.P.; Formal analysis: K.L.-T., N.H., O.B., F.-H.J., P.P., L.J.; Resources: J.S.D., J.H.M.; Writing - original draft: K.L.-T., O.B., J.H.M., L.J.; Writing - review & editing: K.L.-T., O.B., P.P., J.H.M., L.J.; Supervision: L.J.; Project administration: L.J.; Funding acquisition: L.J.

Funding

This work was supported by grants from Canadian Institutes of Health Research (MOP-15139 to L.J.) and Natural Sciences and Engineering Research Council of Canada (NSERC) (194559 to L.J.) and by a NSERC summer studentship (to F.-H.J.).

Supplementary information

Supplementary information available online at
http://dev.biologists.org/lookup/doi/10.1242/dev.152686.supplemental

References

Ackerman, K. G., Vargas, S. O., Wilson, J. A., Jennings, R. W., Kozakewich, H. P. W. and Pober, B. R. (2012). Congenital diaphragmatic defects: proposal for a new classification based on observations in 234 patients. *Pediatr. Dev. Pathol.* **15**, 265-274.

Al Alam, D., El Agha, E., Sakurai, R., Kheirollahi, V., Moiseenko, A., Danopoulos, S., Shrestha, A., Schmoldt, C., Quantius, J., Herold, S. et al. (2015). Evidence for the involvement of fibroblast growth factor 10 in lipofibroblast formation during embryonic lung development. *Development* **142**, 4139-4150.

Allan, D. W. and Greer, J. J. (1997). Embryogenesis of the phrenic nerve and diaphragm in the fetal rat. *J. Comp. Neurol.* **382**, 459-468.

Arora, R., Metzger, R. J. and Papaioannou, V. E. (2012). Multiple roles and interactions of *Tbx4* and *Tbx5* in development of the respiratory system. *PLoS Genet.* **8**, e1002866.

Aubin, J., Lemieux, M., Tremblay, M., Bérard, J. and Jeannotte, L. (1997). Early postnatal lethality in *Hoxa-5* mutant mice is attributable to respiratory tract Defects. *Dev. Biol.* **192**, 432-445.

Aubin, J., Lemieux, M., Moreau, J., Lapointe, J. and Jeannotte, L. (2002). Cooperation of *Hoxa5* and *Pax1* genes during formation of the pectoral girdle. *Dev. Biol.* **244**, 96-113.

Bellusci, S., Grindley, J., Emoto, H., Itoh, N. and Hogan, B. L. (1997). Fibroblast growth factor 10 (FGF10) and branching morphogenesis in the embryonic mouse lung. *Development* **124**, 4867-4878.

Bentzinger, C. F., Wang, Y. X. and Rudnicki, M. A. (2012). Building muscle: molecular regulation of myogenesis. *Cold Spring Harb. Perspect Biol.* **4**, pii: a008342.

Bérubé-Simard, F.-A. and Jeannotte, L. (2014). Hoxa5/Cre transgenic mice: Novel tools for regional deletion along the anterior-posterior axis. *genesis* **52**, 149-156.

Borensztein, M., Monnier, P., Louault, Y., Ripoche, M.-A., Tiret, L., Yao, Z., Tapscott, S. J., Forné, T., Montarras, D. and Dandolo, L. (2013). Myod and *H19-Igf2* locus interactions are required for diaphragm formation in the mouse. *Development* **140**, 1231-1239.

Boucherat, O., Chakir, J. and Jeannotte, L. (2012). The loss of *Hoxa5* function promotes Notch-dependent goblet cell metaplasia in lung airways. *Biol. Open* **1**, 677-691.

Boucherat, O., Montaron, S., Bérubé-Simard, F.-A., Aubin, J., Philippidou, P., Wellik, D. M., Dasen, J. S. and Jeannotte, L. (2013). Partial functional redundancy between *Hoxa5* and *Hoxb5* paralog genes during lung morphogenesis. *Am. J. Physiol. Lung Cell. Mol. Physiol.* **304**, L817-L830.

Boucherat, O., Nadeau, V., Bérubé-Simard, F.-A., Charron, J. and Jeannotte, L. (2014). Crucial requirement of ERK/MAPK signaling in respiratory tract development. *Development* **141**, 3197-3211.

Boucherat, O., Landry-Truchon, K., Aoidi, R., Houde, N., Nadeau, V., Charron, J. and Jeannotte, L. (2017). Lung development requires an active ERK/MAPK pathway in the lung mesenchyme. *Dev. Dyn.* **246**, 72-82.

Braun, T., Rudnicki, M. A., Arnold, H.-H. and Jaenisch, R. (1992). Targeted inactivation of the muscle regulatory gene Myf-5 results in abnormal rib development and perinatal death. *Cell* **71**, 369-382.

Chang, D. R., Martinez Alanis, D., Miller, R. K., Ji, H., Akiyama, H., McCrea, P. D. and Chen, J. (2013). Lung epithelial branching program antagonizes alveolar differentiation. *Proc. Natl. Acad. Sci. USA* **110**, 18042-18051.

Chen, J. W., Zahid, S., Shilts, M. H., Weaver, S. J., Leskowitz, R. M., Habbsa, S., Aronowitz, D., Rokins, K. P., Chang, Y., Pinnella, Z. et al. (2013). Hoxa-5 acts in segmented somites to regulate cervical vertebral morphology. *Mech. Dev.* **130**, 226-240.

Coulombe, Y., Lemieux, M., Moreau, J., Aubin, J., Joksimovic, M., Bérubé-Simard, F.-A., Tabariès, S., Boucherat, O., Guillou, F., Larochelle, C. et al. (2010). Multiple promoters and alternative splicing: *Hoxa5* transcriptional complexity in the mouse embryo. *PLoS ONE* **5**, e10600.

Dessaud, E., Yang, L. L., Hill, K., Cox, B., Ulloa, F., Ribeiro, A., Mynett, A., Novitch, B. G. and Briscoe, J. (2007). Interpretation of the sonic hedgehog morphogen gradient by a temporal adaptation mechanism. *Nature* **450**, 717-720.

Elluru, R. G. and Whitsett, J. A. (2004). Potential role of *Sox9* in patterning tracheal cartilage ring formation in an embryonic mouse model. *Arch. Otolaryngol. Head Neck Surg.* **130**, 732-736.

Geng, Y., Dong, Y., Yu, M., Zhang, L., Yan, X., Sun, J., Qio, L., Geng, H., Nakajima, M., Furuichi, T. et al. (2011). Follistatin-like 1 (Fstl1) is a bone morphogenetic protein (BMP) 4 signaling antagonist in controlling mouse lung development. *Proc. Natl. Acad. Sci. USA* **108**, 7058-7063.

Goss, A. M., Tian, Y., Cheng, L., Yang, J., Zhou, D., Cohen, E. D. and Morrisey, E. E. (2011). Wnt2 signaling is necessary and sufficient to activate the airway smooth muscle program in the lung by regulating myocardin/Mrtf-B and Fgf10 expression. *Dev. Biol.* **356**, 541-552.

Greer, J. J., Allan, D. W., Martin-Caraballo, M. and Lemke, R. P. (1999). An overview of phrenic nerve and diaphragm muscle development in the perinatal rat. *J. Appl. Physiol.* **86**, 779-786.

Hamilton, T. G., Klinghoffer, R. A., Corrin, P. D. and Soriano, P. (2003). Evolutionary divergence of platelet-derived growth factor alpha receptor signaling mechanisms. *Mol. Cell. Biol.* **11**, 4013-4025.

Harfe, B. D., Scherz, P. J., Nissim, S., Tian, H., McMahon, A. P. and Tabin, C. J. (2004). Evidence for an expansion-based temporal Shh gradient in specifying vertebrate digit identities. *Cell* **118**, 517-528.

Herriges, J. C., Yi, L., Hines, E. A., Harvey, J. F., Xu, G., Gray, P. A., Ma, Q. and Sun, X. (2012). Genome-scale study of transcription factor expression in the branching mouse lung. *Dev. Dyn.* **241**, 1432-1453.

Hogan, B. L., Barkauskas, C. E., Chapman, H. A., Epstein, J. A., Jain, R., Hsia, C. C., Niklason, L., Calle, E., Le, A., Randell, S. H. et al. (2014). Repair and regeneration of the respiratory system: complexity, plasticity, and mechanisms of lung stem cell function. *Cell Stem Cells* **15**, 123-138.

Hrycaj, S. M., Dye, B. R., Baker, N. C., Larsen, B. M., Burke, A. C., Spence, J. R. and Wellik, D. M. (2015). *Hox5* genes regulate the Wnt2/2b-Bmp4-signaling axis duringl development. *Cell Rep.* **12**, 903-912.

Jay, P. Y., Bielinska, M., Erlich, J. M., Mannisto, S., Pu, W. T., Heikinheimo, M. and Wilson, D. B. (2007). Impaired mesenchymal cell function in *Gata4* mutant mice leads to diaphragmatic hernias and primary lung defects. *Dev. Biol.* **301**, 602-614.

Jeannotte, L., Lemieux, M., Charron, J., Poirier, F. and Robertson, E. J. (1993). Specification of axial identity in the mouse: role of the *Hoxa-5* (*Hox1. 3*) gene. *Genes Dev.* **7**, 2085-2096.

Jeannotte, L., Gotti, F. and Landry-Truchon, K. (2016). Hoxa5: a key player in development and disease. *J. Dev. Biol.* **4**, 13.

Jung, H. and Dasen, J. S. (2015). Evolution of patterning systems and circuit elements for locomotion. *Dev. Cell* **32**, 408-422.

Kassar-Duchossoy, L., Gayraud-Morel, B., Gomès, D., Rocancourt, D., Buckingham, M., Shinin, V. and Tajbakhsh, S. (2004). Mrf4 determines skeletal muscle identity in *Myf5*:*Myod* double-mutant mice. *Nature* **431**, 466-471.

Kinkead, R., Leblanc, M., Gulemetova, R., Lalancette-Hébert, M., Lemieux, M., Mandeville, I. and Jeannotte, L. (2004). Respiratory adaptations to lung morphological defects in adult mice lacking *Hoxa5* gene function. *Ped. Res.* **56**, 553-562.

Kotecha, S. (2000). Lung growth for beginners. *Paed. Respir. Rev.* **1**, 308-313.

Lefebvre, V., Huang, W., Harley, V. R., Goodfellow, P. N. and de Combrugghe, B. (1997). SOX9 is a potent activator of the chondrocyte-specific enhancer of the Proα1(II) collagen gene. *Mol. Cell. Biol.* **17**, 2336-2346.

Lefebvre, V., Li, P. and de Combrugghe, B. (1998). A new long form of Sox5 (L-Sox5), Sox6 and Sox9 are coexpressed in chondrogenesis and cooperatively activate the type II collagen gene. *EMBO J.* **17**, 5718-5733.

Li, Y., Gordon, J., Manley, N. R., Litingtung, Y. and Chiang, C. (2008). Bmp4 is required for tracheal formation: A novel mouse model for tracheal agenesis. *Dev. Biol.* **322**, 145-155.

Liggins, G. C., Vilos, G. A., Campos, G. A., Kitterman, J. A. and Lee, C. H. (1981). The effect of spinal cord transection on lung development in fetal sheep. *J. Dev. Physiol.* **3**, 267-274.

Lindahl, P., Karlsson, L., Hellström, M., Gebre-Medhin, S., Willetts, K., Heath, J. K. and Betsholtz, C. (1997). Alveogenesis failure in PDGF-A deficient mice is coupled to lack of distal spreading of alveolar smooth muscle cell progenitors during lung development. *Development* **124**, 3943-3953.

Madisen, L., Zwingman, T. A., Sunkin, S. M., Oh, S. W., Zarwala, H. A., Gu, H., Ng, L. L., Palmiter, R. D., Hawrylycz, M. J., Jones, A. R. et al. (2010). A robust and high-throughput Cre reporting and characterization system for the whole mouse brain. *Nat. Neurosci.* **13**, 133-140.

Mandeville, I., Aubin, J., LeBlanc, M., Lalancette-Hébert, M., Janelle, M.-F., Tremblay, G. M. and Jeannotte, L. (2006). Impact of the loss of *Hoxa5* function on lung alveogenesis. *Am. J. Pathol.* **169**, 1312-1327.

McGinnis, W. and Krumlauf, R. (1992). Homeobox genes and axial patterning. *Cell* **68**, 283-302.

Merrell, A. J. and Kardon, G. (2013). Development of the diaphragm–a skeletal muscle essential for mammalian respiration. *FEBS J.* **280**, 4026-4035.

Merrell, A. J., Ellis, B. J., Fox, Z. D., Lawson, J. A., Weiss, J. A. and Kardon, G. (2015). Muscle connective tissue controls development of the diaphragm and is a source of congenital diaphragmatic hernias. *Nat. Genet.* **47**, 496-504.

Miller, M. F., Cohen, E. D., Baggs, J. E., Lu, M. M., Hogenesch, J. B. and Morrisey, E. E. (2012). Wnt ligands signal in a cooperative manner to promote foregut organogenesis. *Proc. Natl. Acad. Sci. USA* **109**, 15348-15353.

Morrisey, E. E. and Hogan, B. L. M. (2010). Preparing for the first breath: genetic and cellular mechanisms in lung development. *Dev. Cell* **18**, 8-23.

Muzumdar, M. D., Tasic, B., Miyamichi, K., Li, L. and Luo, L. (2007). A global double-fluorescent Cre reporter mouse. *Genesis* **45**, 593-605.

Park, G.-H., Maeno-Hikichi, Y., Awano, T., Landmesser, L. T. and Monani, U. R. (2010a). Reduced survival of motor neuron (SMN) protein in motor neuronal progenitors functions cell autonomously to cause spinal muscular atrophy in model mice expressing the human centromeric (*SMN2*) gene. *J. Neuro.* **30**, 12005-12019.

Park, J., Zhang, J. J. R., Moro, A., Kushida, M., Wegner, M. and Kim, P. C. W. (2010b). Regulation of *Sox9* by Sonic Hedgehog (*Shh*) is essential for patterning and formation of tracheal cartilage. *Dev. Dyn.* **239**, 514-526.

Philippidou, P., Walsh, C. M., Aubin, J., Jeannotte, L. and Dasen, J. S. (2012). Sustained *Hox5* gene activity is required for respiratory motor neuron development. *Nat. Neurosci.* **15**, 1636-1644.

Polla, B., D'Antona, G., Bottinelli, R. and Reggiani, C. (2004). Respiratory muscle fibres: specialisation and plasticity. *Thorax* **59**, 808-817.

Rudnicki, M. A., Schnegelsberg, P. N. J., Stead, R. H., Braun, T., Arnold, H.-H. and Jaenisch, R. (1993). MyoD or Myf-5 is required for the formation of skeletal muscle. *Cell* **75**, 1351-1359.

Sala, F. G., Del Moral, P.-M., Tiozzo, C., Alam, D. A., Warburton, D., Grikscheit, T., Veltmaat, J. M. and Bellusci, S. (2011). FGF10 controls the patterning of the tracheal cartilage rings via Shh. *Development* **138**, 273-282.

Sambasivan, R. and Tajbakhsh, S. (2007). Skeletal muscle stem cell birth and properties. *Sem. Cell. Dev. Biol.* **18**, 870-882.

Schiaffino, S. and Reggiani, C. (2011). Fiber types in mammalian skeletal muscles. *Physiol. Rev.* **91**, 1447-1531.

Seale, P., Sabourin, L. A., Girgis-Gabardo, A., Mansouri, A., Gruss, P. and Rudnicki, M. A. (2000). Pax7 is required for the specification of myogenic satellite cells. *Cell* **102**, 777-786.

Shu, W., Guttentag, S., Wang, Z., Andl, T., Ballard, P., Lu, M. M., Piccolo, S., Birchmeier, W., Whitsett, J. A., Millar, S. E. et al. (2005). Wnt/beta-catenin signaling acts upstream of N-myc, BMP4, and FGF signaling to regulate proximal-distal patterning in the lung. *Dev. Biol.* **283**, 226-239.

Soriano, P. (1999). Generalized lacZ expression with the ROSA26 Cre reporter strain. *Nature Genet.* **21**, 70-71.

Tabariès, S., Lemieux, M., Aubin, J. and Jeannotte, L. (2007). Comparative analysis of *Hoxa5* allelic series. *genesis* **45**, 218-228.

Tajbakhsh, S., Rocancourt, D., Cossu, G. and Buckingham, M. (1997). Redefining the genetic hierarchies controlling skeletal myogenesis: Pax-3 and Myf-5 act upstream of MyoD. *Cell* **89**, 127-138.

Tian, Y., Zhang, Y., Hurd, L., Hannenhalli, S., Liu, F., Lu, M. M. and Morrisey, E. E. (2011). Regulation of lung endoderm progenitor cell behavior by miR302/367. *Development* **138**, 1235-1245.

Development (2017) 144, 3547-3561 doi:10.1242/dev.152686

Tremblay, P., Dietrich, S., Mericskay, M., Schubert, F. R., Li, Z. and Paulin, D. (1998). A crucial role for Pax3 in the development of the hypaxial musculature and the long-range migration of muscle precursors. *Dev. Biol.* **203**, 49-61.

Turcatel, G., Rubin, N., Menke, D. B., Martin, G., Shi, W. and Warburton, D. (2013). Lung mesenchymal expression of Sox9 plays a critical role in tracheal development. *BMC Biol.* **11**, 117.

Umansky, K. B., Gruenbaum-Cohen, Y., Tsoory, M., Feldmesser, E., Goldenberg, D., Brenner, O. and Groner, Y. (2015). Runx1 transcription factor is required for myoblasts proliferation during muscle regeneration. *PLoS Genet.* **11**, e1005457.

Wang, X., Blagden, C., Fan, J., Nowak, S. J., Taniuchi, I., Littman, D. R. and Burden, S. J. (2005). Runx1 prevents wasting, myofibrillar disorganization, and autophagy of skeletal muscle. *Genes Dev.* **19**, 1715-1722.

Wigglesworth, J. S. and Desai, R. (1979). Effects on lung growth of cervical cord section in the rabbit fetus. *Early Human Dev.* **3**, 51-65.

Yu, K., Xu, J., Liu, Z., Sosic, D., Shao, J., Olson, E. N., Towler, D. A. and Ornitz, D. M. (2003). Conditional inactivation of FGF receptor 2 reveals an essential role for FGF signaling in the regulation of osteoblast function and bone growth. *Development* **130**, 3063-3074.

Zhu, X., Yeadon, J. E. and Burden, S. J. (1994). AML1 is expressed in skeletal muscle and is regulated by innervation. *Mol. Cell. Biol.* **14**, 8051-8057.

SUPPLEMENTAL DATA

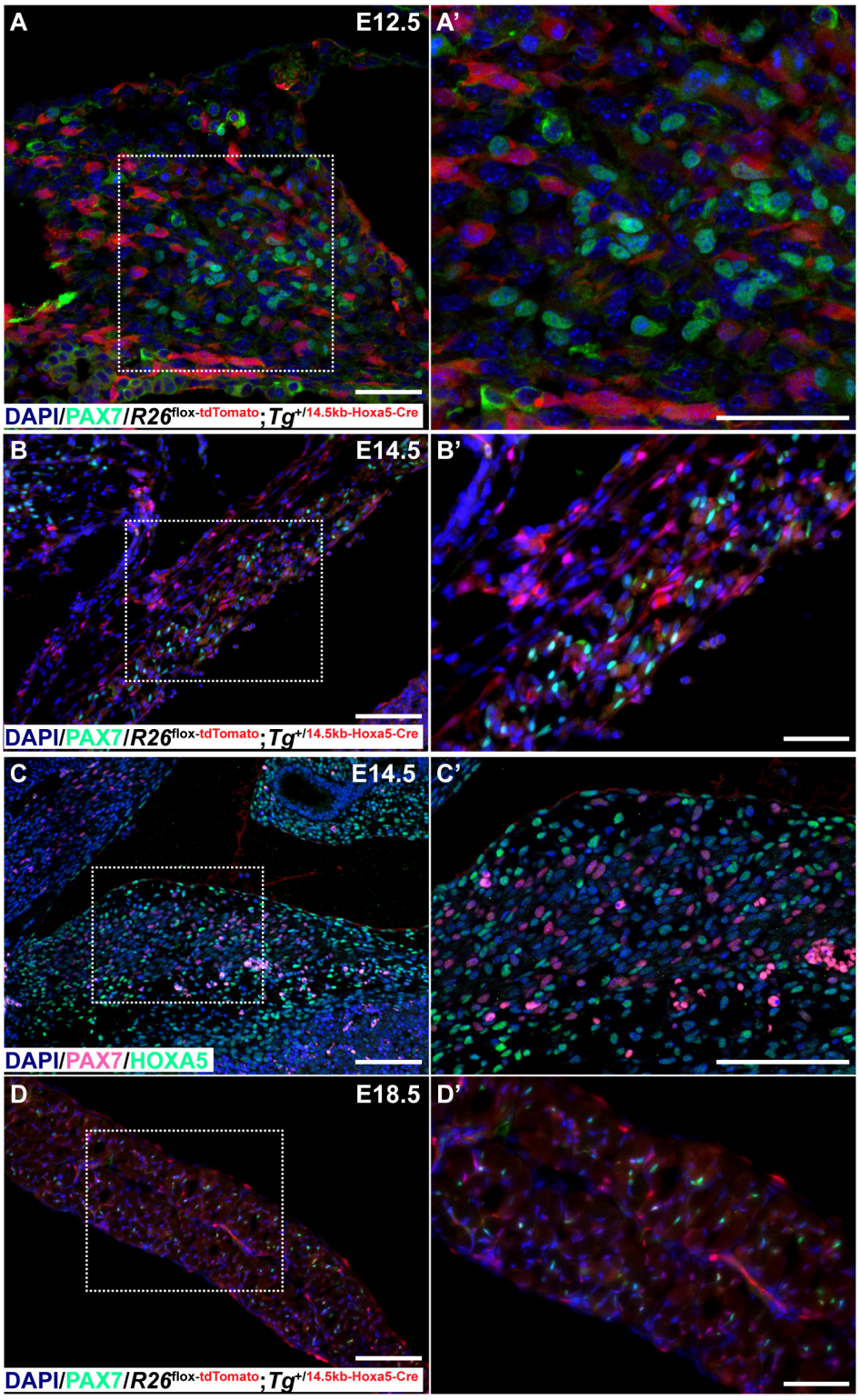

Figure S1

Figure S1. *Hoxa5* is not expressed in muscle cells of the diaphragm. PAX7 immunostaining was performed on sections of the developing diaphragm from E12.5 (A-A'), E14.5 (B-B') and E18.5 (D-D') *R26*^{mT};*Hoxa5-Cre* embryos. No PAX7 co-staining was observed in *Hoxa5* descendant cells (*R26*^{mT}-positive). PAX7 and HOXA5 co-immunolabelling was also performed on diaphragm sections from E14.5 wt embryos and no co-staining was observed (C-C'). Scale bars: 100 µm (B,D), 50 µm (B',C-C',D'), 25 µm (A-A').

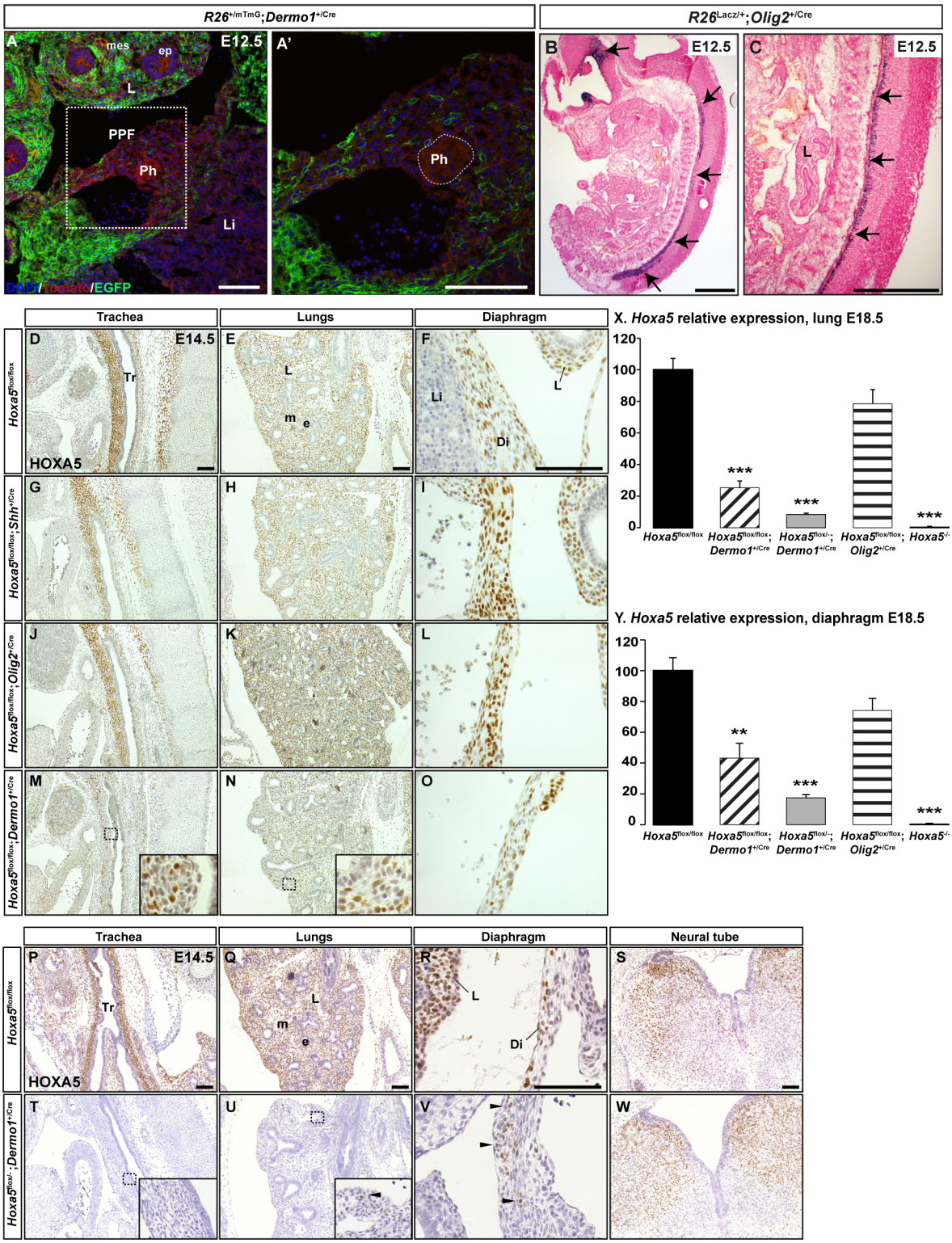

Figure S2

Figure S2. Cre recombinase specificity and efficiency of the *Hoxa5* deletion by the *Shh*^{Cre} , *Dermo1*^{Cre} and *Olig2*^{Cre} alleles in the developing respiratory system. Validation of Cre specificity was assessed by breeding *Dermo1*$^{+/Cre}$ and *Olig2*$^{+/Cre}$ mice with *R26*$^{mT/mG}$ and *R26*$^{+/LacZ}$ reporter mice, respectively. Dermo1Cre activity was assayed by GFP visualization on sections of E12.5 *R26*$^{mT/mG}$;*Dermo1*$^{+/Cre}$ embryos (A-A'). Olig2Cre activity was monitored by β-galactosidase staining in sections of E12.5 *R26*$^{+/LacZ}$;*Olig2*$^{+/Cre}$ embryos (B,C). Efficiency of the *Hoxa5* deletion with the *Shh*^{Cre}, *Dermo1*^{Cre} and *Olig2*^{Cre} alleles in the developing trachea, lung and diaphragm was tested by IHC at E14.5 (D-W). As expected, HOXA5 mesenchymal expression was not affected by ShhCre and Olig2Cre recombinases (G-L), whereas the efficiency of the Dermo1Cre was incomplete and residual HOXA5 expression remained (M-O, P-W). Efficiency of the *Hoxa5* deletion in lung and diaphragm was also monitored by qRT-PCR at E18.5 (X-Y). A significant 75% and 57% reduction was observed in *Hoxa5*$^{flox/flox}$;*Dermo1*$^{+/Cre}$ lung and diaphragm, respectively. The reduction was more important in *Hoxa5*$^{flox/-}$;*Dermo1*$^{+/Cre}$ specimens. No significant variation was seen in E18.5 *Hoxa5*$^{flox/flox}$;*Olig2*$^{+/Cre}$ lungs and diaphragm but a complete loss of *Hoxa5* expression was measured in *Hoxa5*$^{-/-}$ specimens. Di, diaphragm; ep, epithelium; L, lungs; Li, liver; mes, mesenchyme; Ph, phrenic nerve; Tr, trachea. Scale bars: 1 mm (B,C), 100 μm (D-W), 50 μm (A-A').

A. Ratio of genotypes of offspring from *Hoxa5*$^{flox/+}$;*Shh*$^{+/Cre}$ x *Hoxa5*$^{flox/flox}$

			Shh $^{+/+}$		*Shh* $^{+/Cre}$	
Age	**# of litters**	**# of animals**	***Hoxa5*** $^{flox/+}$	***Hoxa5*** $^{flox/flox}$	***Hoxa5*** $^{flox/+}$	***Hoxa5*** $^{flox/flox}$
E18.5	9	59 (100%)	12 (21%)	15 (25%)	15 (25%)	17 (29%)
P30	7	47 (100%)	10 (21%)	17 (36%)	7 (15%)	13 (28%)
% Expected			**25%**	**25%**	**25%**	**25%**

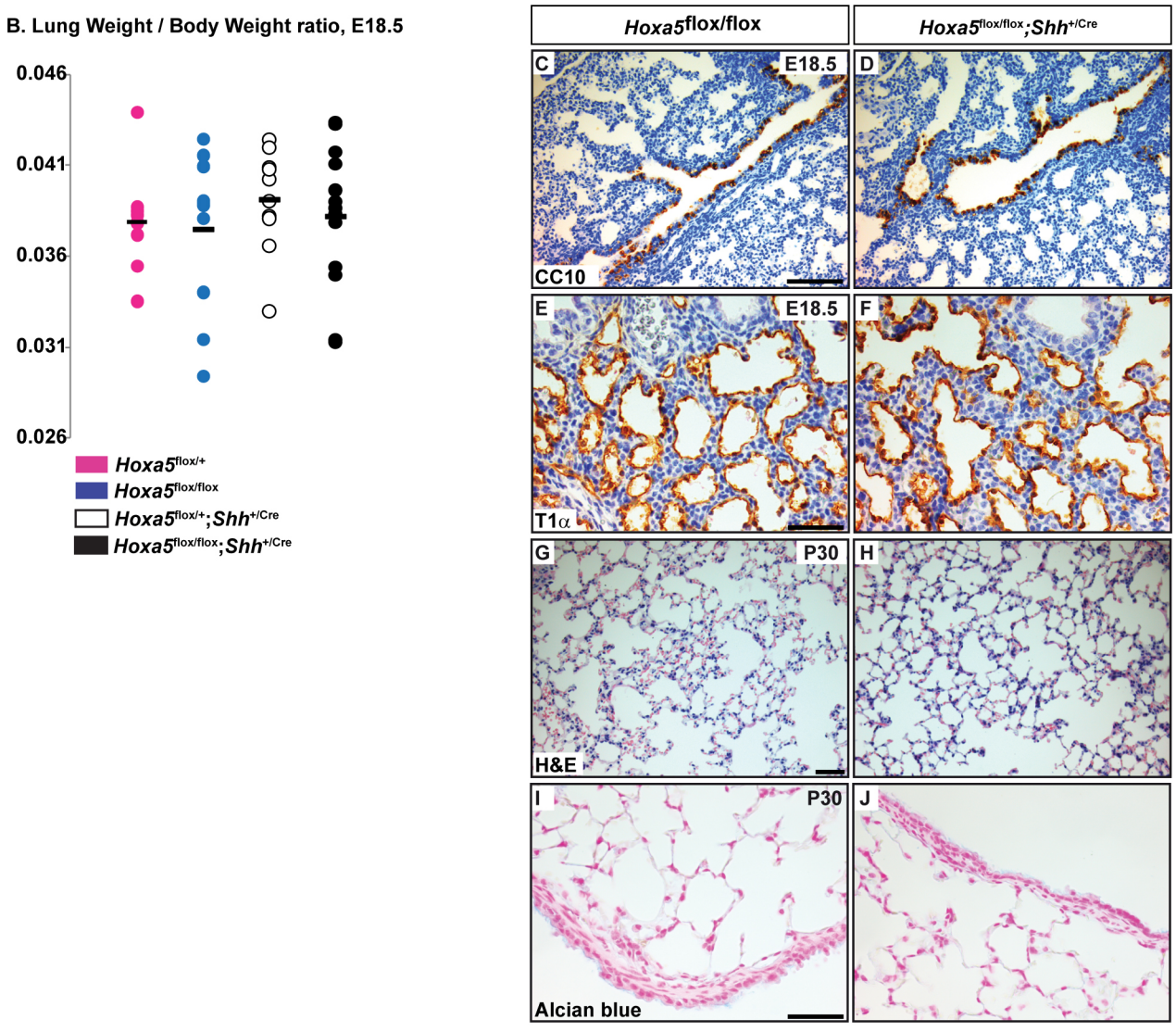

Figure S3

Figure S3. No lung phenotype is caused by the epithelial *Hoxa5* inactivation. Expected mendelian ratios of genotypes of offspring resulting from breeding of *Hoxa5*$^{flox/flox}$ with *Hoxa5*$^{flox/+}$;*Shh*$^{+/cre}$ mice (A). No change was observed for the LW/BW ratio between *Hoxa5*$^{flox/flox}$;*Shh*$^{+/cre}$ embryos and controls at E18.5 (B). No abnormal epithelial cell differentiation of club cells and type I pneumocytes was seen along the respiratory tract of E18.5 *Hoxa5*$^{flox/flox}$;*Shh*$^{+/cre}$ embryos, as assessed by immunostaining for CC10 and T1a, respectively (C-F). Alveolar surface density was normal and no goblet cell metaplasia was detected in lungs from *Hoxa5*$^{flox/flox}$;*Shh*$^{+/cre}$ adults (G-J). These data reflected the lack of *Hoxa5* cell-autonomous function in lung epithelium. Scale bars: 100 µm (C,D,G,H), 50 µm (E,F,I,J).

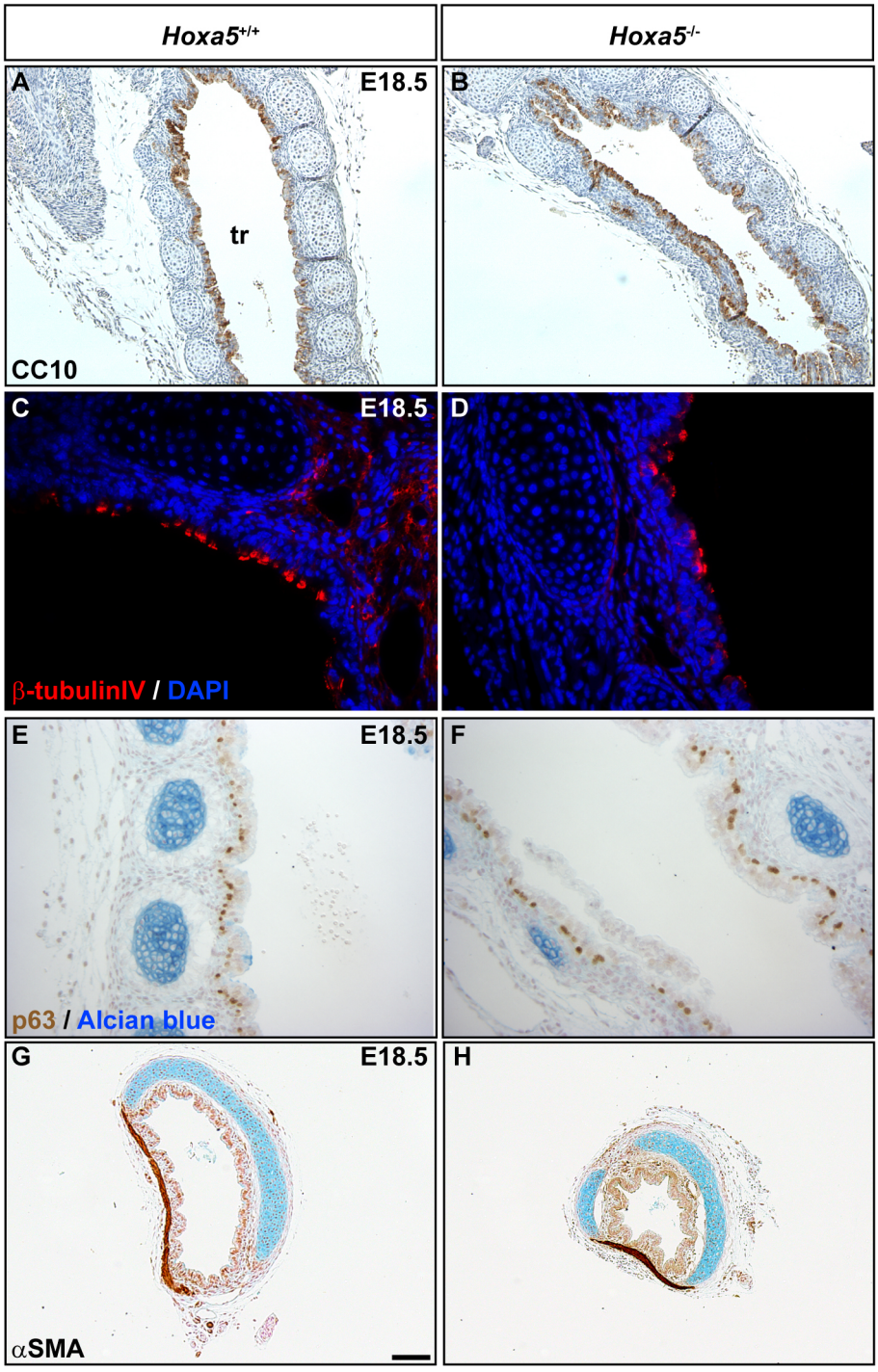

Figure S4

Figure S4. Tracheal smooth muscle formation and epithelial differentiation are unchanged in *Hoxa5*$^{-/-}$ embryos. No quantitative and qualitative variation in club, ciliated, basal, goblet and smooth muscle cells was observed in E18.5 *Hoxa5*$^{-/-}$ tracheas, as assessed by immuno- and histological stainings for CC10, β-tubulinIV, p63, Alcian blue and αSMA, respectively (A-H).

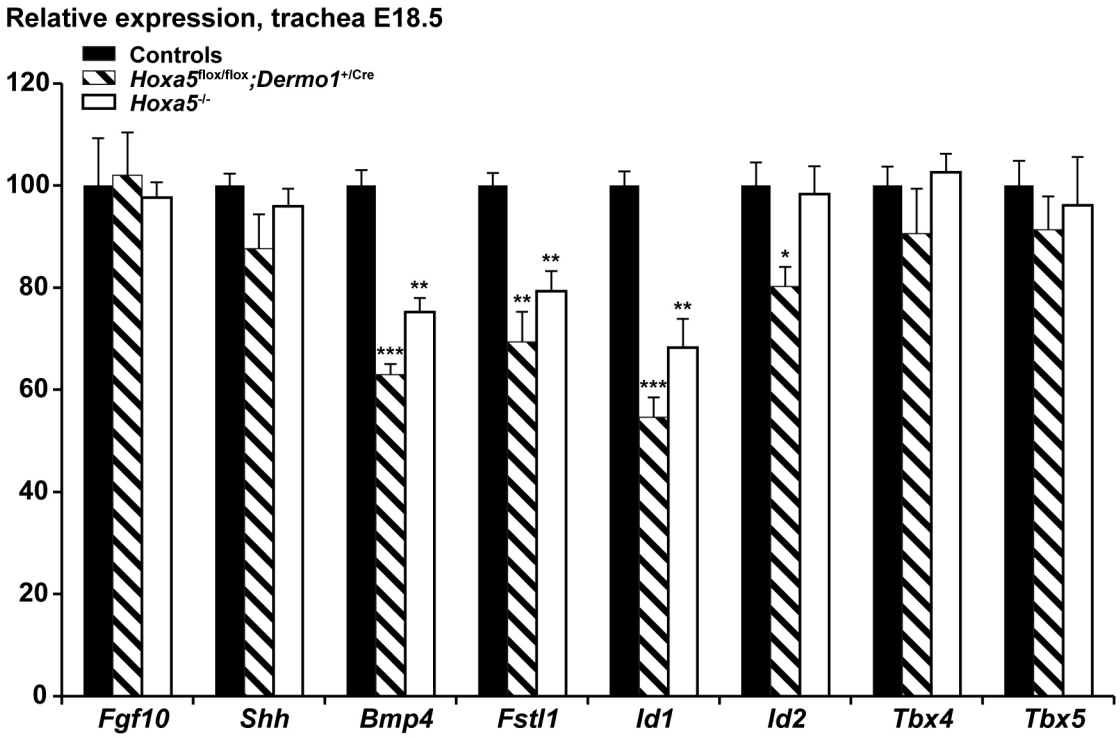

Figure S5

Figure S5. Impact of the loss of *Hoxa5* function on the expression of regulators of tracheal cartilage formation. qRT-PCR analysis of *Fgf10*, *Shh, Bmp4, Fstl1*, *Id1*, *Id2*, *Tbx4* and *Tbx5* expression levels in tracheas from E18.5 wt, *Hoxa5*$^{flox/flox}$;*Dermo1*$^{+/Cre}$ and *Hoxa5*$^{-/-}$ embryos.

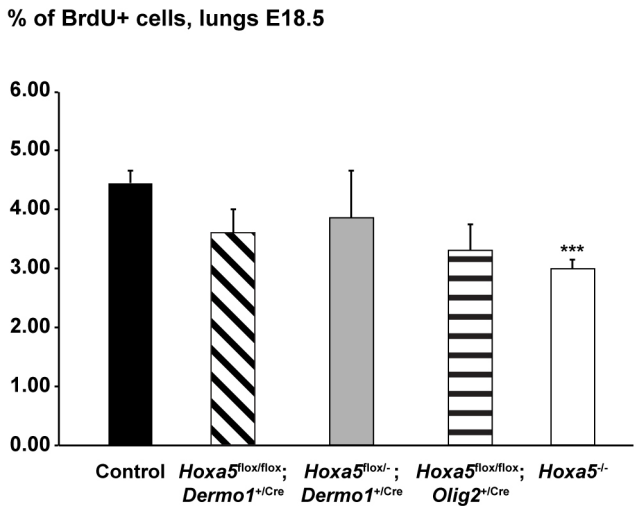

Figure S6

Figure S6. *Hoxa5* mesenchymal and motor neuron mutations differentially influence proliferation of the developing lung. Percentage of BrdU+ cells revealed a downward trend in cell proliferation in E18.5 *Hoxa5*$^{flox/flox}$;*Dermo1*$^{+/Cre}$, *Hoxa5*$^{flox/-}$;*Dermo1*$^{+/Cre}$ and *Hoxa5*$^{flox/flox}$;*Olig2*$^{+/Cre}$ lungs and a significant reduction in *Hoxa5*$^{-/-}$ mutants compared to controls.

A. Relative expression, Lungs E12.5

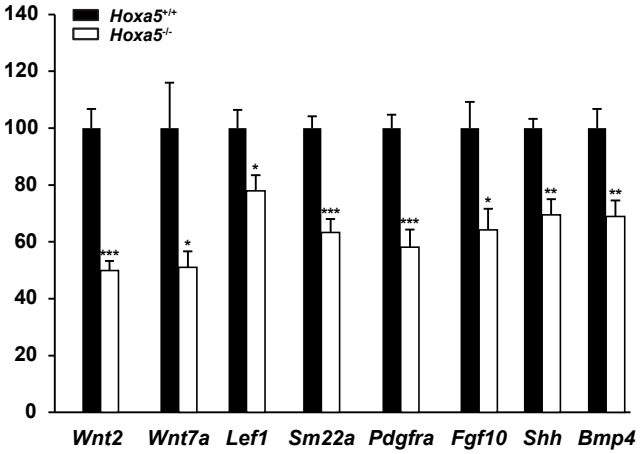

B. Relative expression, Lungs E18.5

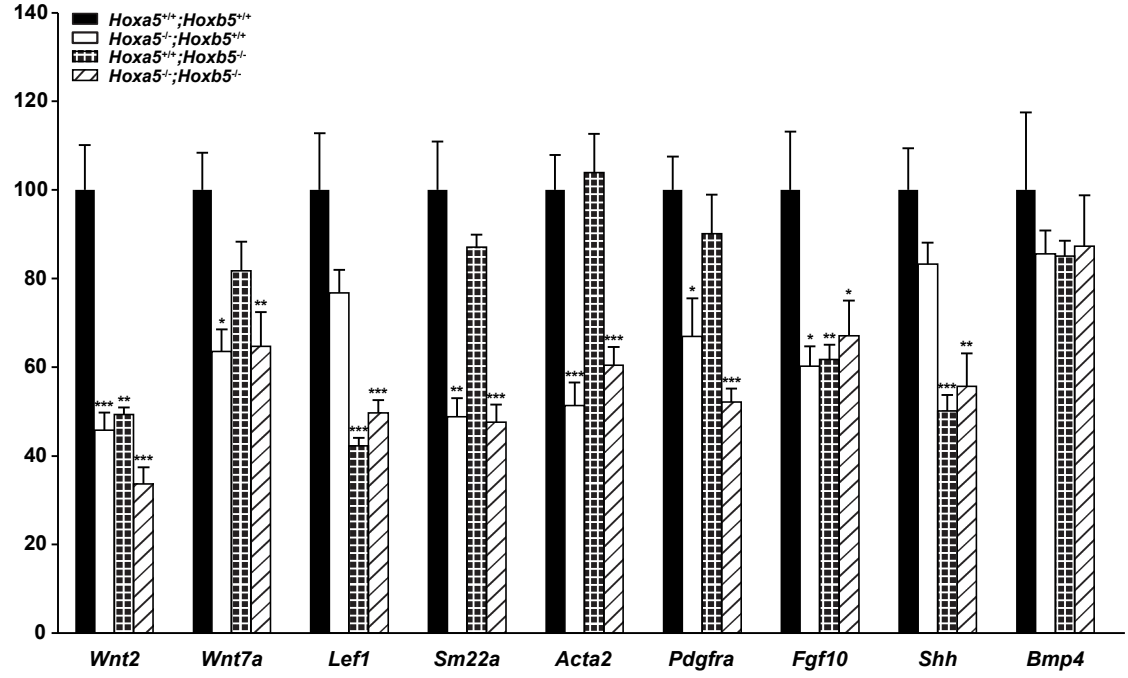

C. Relative expression, Lungs E18.5

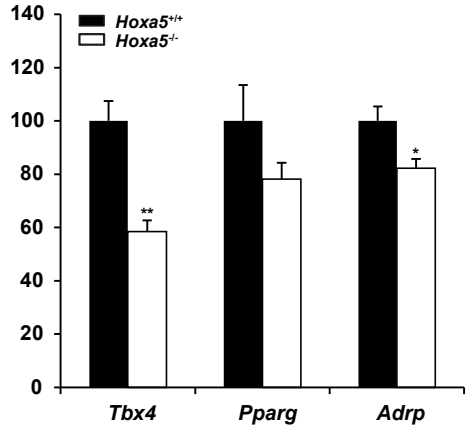

Figure S7. Specific contribution of *Hoxa5* in the control of lung signaling pathways. Expression levels of *Wnt2, Wnt7a, Lef1, Sm22a, Pdgfra, Fgf10, Shh* and *Bmp4* genes in lungs from E12.5 wt and *Hoxa5*$^{-/-}$ embryos (A). All these genes showed a significantly decreased expression in *Hoxa5*$^{-/-}$ lungs. Expression levels of *Wnt2, Wnt7a, Lef1, Sm22a, aSma, Pdgfra, Fgf10, Shh* and *Bmp4* genes in lungs from E18.5 wt, *Hoxa5*$^{-/-}$, *Hoxb5*$^{-/-}$ and *Hoxa5*$^{-/-}$;*Hoxb5*$^{-/-}$ compound mutant embryos (B). *Hoxa5*$^{-/-}$ specimens showed significantly reduced expression levels for *Wnt2, Wnt7a, Sm22a, aSma, Pdgfra* and *Fgf10* while *Hoxb5*$^{-/-}$ specimens showed decreased expression levels for *Wnt2, Lef1, Fgf10* and *Shh.* In *Hoxa5*$^{-/-}$;*Hoxb5*$^{-/-}$ compound mutants, except for *Bmp4*, all genes tested showed a significant reduced expression. Expression levels of *Tbx4*, *Pparg* and *Adrp* genes in lungs from E18.5 wt and *Hoxa5*$^{-/-}$ embryos (C). *Tbx4* and *Adrp* genes showed a significantly decreased expression in *Hoxa5*$^{-/-}$ lungs, while *Pparg* showed a downward trend.

Supplementary Table 1. List of primary and secondary antibodies

Antigen	Antibody/clone	Reference	Source	Dilution
AQP5 (Aquaporin 5)	rabbit polyclonal	Ab78486	Abcam, Toronto, ON, Canada	1:400
αSMA	rabbit polyclonal	Ab5694	Abcam, Toronto, ON, Canada	1:300
BrdU	mouse monoclonal/ clone 131-14871	MAB4072	Millipore, Billerica, MA, USA	1:1000
α-bungarotoxin, Alexa Fluor 555 conjugate		B35451	Invitrogen, Carlsbad, CA, USA	1:1000
βIV-Tubulin	Mouse monoclonal clone ONS1A6	MU178-UC	Biogenex, Fremont, CA, USA	1:150
CC10	goat polyclonal		Gift from Dr. G. Singh, Pittsburg, PA, USA	1:400
Collagen Type II	Mouse/clone II-II6B3. Supernatant		Hybridoma Bank, IO, USA	1:75
HOXA5	rabbit polyclonal	HPA029319	Sigma Aldrich, Oakville, ON, Canada	1:1000
HOXA5	rabbit polyclonal		From Dr. J. Dasen, NY, USA	1:10000
α-Laminin	rabbit polyclonal	BRL#6265SA	Gift from Dr. N. Marceau, Qc, Canada	1:50
Neurofilament (NF)	rabbit polyclonal	AB1987	Millipore, Billerica, MA, USA	1:1000
PAX7	mouse monoclonal		Hybridoma Bank, IO, USA	1:10
p63	mouse monoclonal clone 4A4	Sc-8431	Santa Cruz, Santa Cruz, CA, USA	1 :100
RFP (DsRed)	rabbit polyclonal	600-401-379	Rockland, Limerick, PA, USA	1: 200
SOX9	rabbit polyclonal	sc-20095	Santa Cruz, Santa Cruz, CA, USA	1:100
Synaptophysin (SYN)	rabbit polyclonal	08-0130	Invitrogen, Carlsbad, CA, USA	1:5
T1α	syrian-hamster/ clone 8.1.1. Supernatant		Hybridoma Bank, IO, USA	1:75
Biotinylated goat anti-rabbit		BA-1000	Vector Laboratories, Burlington, ON, Canada	1:250
Biotinylated swine anti-goat		CLCC50015	Cedarlane, Burlington, ON, Canada	1:250
Biotinylated goat anti-syrian hamster		107-065-142	Cedarlane, Burlington, ON, Canada	1:250
Biotinylated goat anti-mouse		115-065-003	Cedarlane, Burlington, ON, Canada	1:500
Donkey anti-rabbit, Alexa Fluor 488 conjugate		A-21206	Invitrogen, Carlsbad, CA, USA	1:1000
Goat anti-mouse, Alexa Fluor 647 conjugate		A-21236	Invitrogen, Carlsbad, CA, USA	1:500
Goat anti-rabbit, Alexa Fluor 488 conjugate		A11008	Molecular Probes, Eugene, OR, USA	1:250
TSA Cyanine 3 Plus Evaluation Kit		NEL744E001KT	PerkinElmer, MA, USA	1:50

Supplementary Table 2. List of primer sequences

Gene	Sequence (5'-3')	Fragment size (bp)
Acta2 (aSma)	F-ACAGCTATGTGGGGGATGAA R-GTTGGCCTTAGGGTTCAGTG	194
Adrp (Plin2)	F-GTCCCTCAGCTCTCCTGTTA R-ATAAGCGGAGGACACAAGGT	146
Bmp4	F-AGCGTCCCGCCAGCCGA R-CGGAGCTCTGCCGAGGAG	148
Col2a1	F-TGGGAATGTCCTCTGCGATG R-TGCCCCTTTGGCCCTAATTT	135
Fgf10	F- TCAAAGCCATCAACAGCAACTATT R-CTCTTTCAGCTTACAGTCGTTGTTAAA	95
Fstl1	F-ATGGCGACTCTCACCTGGAC R-CAATGAGGGCGTCAACACAG	135
Hoxa5	F- CCCAGATCTACCCCTGGATG R- GGCATGAGCTATTTCGATCCT	173
Igf2	F- CCGTACTTCCGGACGACTT R- ATCAGGGGACGATGACGTTT	181
Id1	F-CATGAACGGCTGCTACTCAC R-GAACACATGCCGCCTCG	236
Id2	F-CCTGCATCACCAGAGACCTG R-GGGAATTCAGATGCCTGCAA	102
Lef1	F-AAATGGGTCCCTTTCTCCAC R-CTCGTCGCTGTAGGTGATGA	107
Myf5	F- CCCACCTCCAACTGCTCT R- GCAATCCAAGCTGGACACG	144
Myf6 (Mrf4)	F- ACCCCTACAGCTACAAACCC R- TGCTCCTCCTTCCTTAGCAG	131
Myh1	F- CCGAAGGCGGAACTACTGTAA R- CAGGCTGCATAACGCTCTTT	148
Myh2	F- CAGTGTCTAAGGGCCAAGGGA R- GCCTGGAAAATTCACCGGAT	159
Myh3	F- TTCGCTACAACAGATGCGGA R- CTGGGGTCTTGGTTTCGTTG	175
Myh4	F- TGCTTACGTCAGTCAAGGTGAA R- CATCTGCACTGAATCCCAGG	104
Myh7	F- GGTGGATGATCTGGAGGGAT R- GAGTGCATTTAACTCAAAGTCCTTC	181
Myh8	F- TGAGGAGGCTGAGGAACAATC R- TTACTCTGCGCTGATTTTGGT	160
Myod1 (Myod)	F- GCTCTGATGGCATGATGGATTA R- TGGAGATGCGCTCCACTATG	165
Myog	F- GCCATCCAGTACATTGAGCG R- GTGGGAGTTGCATTCACTGG	123
Pax3	F- GGCGGCAGCAAACCC R- AGGGCACAGTGTTCCGAT	145
Pax7	F- ATTAGCCGAGTGCTCAGAATCA R- CCCTCATCCAGACGGTTCC	140
Pdgfra	F- CCATGCAGTTGCCTTACGACT R- AGAGCCTGCTTTTCACTAGACC	193
Runx1	F- ATGGCAGGCAACGATGAAAA R- AGACGGTGATGGTCAGAGTG	142
Pparg	F-GCCGAGTCTGTGGGGATAAA R-AGGCACTTCTGAAACCGACA	181
Shh	F-TGACTCAGAGGTGCAAAGACA R-ACTCCTCTGAATGATGGCCG	120
Sox5	F-CACCCTGAAGCAGAGGAAGA R-GGCTCTCAGGAGTCCCTTTT	152
Sox6	F-AATTCTTCAGGCCTTCCCTGAC R-CTTAGCCGGGCCTGTTCTTC	219
Sox9	F-GTCGGTGAAGAACGGACAAG R-CTGAGATTGCCCAGAGTGCT	157
Tagln (Sm22a)	F-TGGCTGAAGAATGGTGTGATTC R-TTGAGCCACCTGTTCCATCT	126
Tbx4	F-TCCTACCAGAACCACAAGATCAC R-CCCATTCTCATACTGGTAGTGC	240
Tbx5	F-CCGGAGACAGCTTTTATCGC R-ACTCTTTACTTTGCATCCGAGAC	145
Wnt2	F-TGATGTAGACGCAAGGGGG R-GCCACCTGTAGCTCTCATGTA	129
Wnt7a	F-CACAATAACGAGGCGGGTC R-TCCAGCACGTCTTAGTGGTA	100